A&A 625, A51 (2019)
https://doi.org/10.1051/0004-6361/201732197

Astronomy & Astrophysics

The VIMOS Ultra-Deep Survey: evidence for AGN feedback in galaxies with CIII]-λ1908 Å emission 10.8 to 12.5 Gyr ago⋆

O. Le Fèvre[1], B. C. Lemaux[1,2], K. Nakajima[3,4], D. Schaerer[3,5], M. Talia[6], G. Zamorani[7], P. Cassata[5], B. Garilli[8], D. Maccagni[8], L. Pentericci[9], L. A. M. Tasca[1], E. Zucca[7], R. Amorin[9,14], S. Bardelli[7], A. Cimatti[6], M. Giavalisco[10], L. Guaita[11], N. P. Hathi[12], F. Marchi[9], E. Vanzella[7], D. Vergani[9], and J. Dunlop[13]

[1] Aix Marseille Université, CNRS, LAM (Laboratoire d'Astrophysique de Marseille), UMR 7326, 13388 Marseille, France
e-mail: olivier.lefevre@lam.fr
[2] Department of Physics, University of California, Davis, One Shields Ave., Davis, CA 95616, USA
[3] Geneva Observatory, University of Geneva, ch. des Maillettes 51, 1290 Versoix, Switzerland
[4] European Southern Observatory, 85748 Garching bei Munchen, Germany
[5] Institut de Recherche en Astrophysique et Planétologie – IRAP, CNRS, Université de Toulouse, UPS-OMP, 14, Avenue E. Belin, 31400 Toulouse, France
[6] University of Bologna, Department of Physics and Astronomy (DIFA), V.le Berti Pichat 6/2 40127 Bologna, Italy
[7] INAF–Osservatorio Astronomico di Bologna, Via Ranzani 1-40127 Bologna, Italy
[8] INAF–IASF Milano, Via Bassini 15, 20133 Milano, Italy
[9] INAF–Osservatorio Astronomico di Roma, Via di Frascati 33, 00040 Monte Porzio Catone, Italy
[10] Astronomy Department, University of Massachusetts, Amherst, MA 01003, USA
[11] Núcleo de Astronomía, Facultad de Ingeniería, Universidad Diego Portales, Av. Ejército 441, Santiago, Chile
[12] Space Telescope Science Institute, 3700 San Martin Drive, Baltimore, MD 21218, USA
[13] SUPA, Institute for Astronomy, University of Edinburgh, Royal Observatory, Edinburgh EH9 3HJ, UK
[14] Kavli Institute for Cosmology, University of Cambridge, Madingley Road, Cambridge CB3 0HA, UK

Received 29 October 2017 / Accepted 18 March 2019

ABSTRACT

We analyze the CIII]-λ1908 Å emission properties in a sample of 3899 star-forming galaxies (SFGs) at $2 < z < 3.8$ drawn from the VIMOS Ultra-Deep Survey (VUDS). We find a median rest-frame equivalent width EW(CIII]) = 2.0 ± 0.2 to 2.2 ± 0.2 Å for the whole SFG population at $2 < z < 3$ and $3 < z < 4$, respectively. About 24% of SFGs are showing EW(CIII]) > 3 Å, including ∼20% with modest emission 3 < EW(CIII]) < 10 Å and ∼4% with strong emission EW(CIII]) >10 Å. A small but significant fraction of 1.2% of SFGs presents strong CIII] emission 20 < EW(CIII]) < 40 Å; the four strongest emitters (EW(CIII]) > 40 Å up to ∼95 Å) are associated with broad-line AGN. While this makes CIII] the second most frequent emission line in the UV rest-frame spectra of SFGs after Lyman-α, this line alone cannot be considered an efficient substitute for measuring a galaxy redshift in the absence of Lyα emission, unless the spectral resolution is $R > 3000$ to distinguish among different possible doublets. We find a large dispersion in the weak correlation between EW(CIII]) and EW(Lyα), with galaxies showing strong CIII] and no Lyα, and vice versa. The spectra of SFGs with 10 < EW(CIII]) < 40 Å present strong emission lines that include CIV-λ1549, HeII-λ1640, and OIII-λ1664, but also weaker emission features of highly ionized elements such as SiIV-λ1403, NIV-λ1485, NIII-λ1750, or SiIII-λ1888, indicating the presence of a hard radiation field. We present a broad range of observational evidence supporting the presence of AGN in the strong CIII] emitting population. As EW(CIII]) is rising, we identify increasingly powerful outflows with velocities up to 1014 km s^{-1}; this is beyond what stellar winds are commonly producing. The strongest CIII] emitters are preferentially located below the main sequence of star-forming galaxies; the median star formation rate is reduced by a factor of two. In addition, we find that the median stellar age of the strongest emitters is ∼0.8 Gyr, which is about three times that of galaxies with EW(CIII]) < 10 Å. X-ray stacked imaging of the strong CIII] emitters sample show a marginal 2σ detection that is consistent with low-luminosity AGN $\log(L_X(2-10\,\mathrm{keV})) \sim 42.9\,\mathrm{erg\,s^{-1}}$. Previously presented spectral line analysis and classification support that the strongest emitters require the presence of an AGN. We conclude that this complementary set of evidence is indicative of significant AGN feedback acting in SFGs at $2 < z < 3.8$, and it strongly contributes to star formation quenching. We find that quenching timescales of $\sim 0.25-0.5 \times 10^9$ years are necessary for this AGN feedback to turn part of the star-forming galaxy population with $M_{\mathrm{star}} > 10^{10}\,M_\odot$ at $z \sim 3$ into the population of quiescent galaxies observed at redshift $z \sim 1-2$.

Key words. Galaxy: evolution – galaxies: formation – galaxies: high-redshift – galaxies: star formation

1. Introduction

Progress in understanding the formation and early assembly of galaxies requires assembling large samples of high-redshift galaxies. The first galaxies that formed during the epoch of reionization (EoR) are thought to contribute most of the photons that transform neutral hydrogen into a fully ionized medium at $z > 6$ (Robertson et al. 2015). However, this evidence is based mostly on a census of galaxies that were identified based on their photometric properties (e.g., Bouwens et al. 2015), while confirming their redshift remains difficult because spectral signatures that would allow identifying them are scarce

⋆ Based on data obtained with the European Southern Observatory Very Large Telescope, Paranal, Chile, under Large Program 185.A–0791.

(Pentericci et al. 2011; Stark et al. 2010). Transforming the large population of galaxy candidates at $z > 6$ into reference samples with the confirmed spectroscopic redshifts that are required to infer their physical properties remains a great problem.

In the rest-frame UV spectra of galaxies that are observed at these redshifts, several spectral features are expected to be present, but only a few emission lines may reach sufficient strength to be detected, and either serve as a useful reference for a robust redshift measurement or as a physical diagnostic to the ionizing field and interstellar medium (ISM). The properties of these lines need to be well understood to make progress in finding and characterizing galaxies at these redshifts.

The main spectral features used to identify distant galaxies rely on the properties of the hydrogen atom between the Lyman-α (hereafter Lyα) transition at λ1215.7 Å and the Lyman limit at λ912 Å. While the Lyman limit and continuum drop-out from absorption by gas clouds in the intergalactic medium (IGM) on the line of sight allow identifying candidate high-redshift galaxies from photometry alone, the key feature that allows robustly identifying distant galaxies from spectroscopic follow-up is the Lyα emission. This emission is primarily produced by gas that is photoionized by young hot stars. Lyα emission, when present, is easier to detect than a continuum break, and therefore most of the galaxies at $z > 6$ that are securely confirmed from spectroscopy today are based on the detection of Lyα in emission. Narrow-band imaging is also used for Lyα emitter searches (e.g., Ouchi et al. 2008), but it remains difficult to analyze extreme populations such as strong emitters that appear as massive and old and have little star formation (Taniguchi et al. 2015) without spectral information in addition to Lyα.

Unfortunately, it appears that the fraction of Lyα emitters, while rising up to $z \sim 6$ (e.g., Stark et al. 2009; Cassata et al. 2015; De Barros et al. 2017), seems to suddenly decrease at higher redshifts. This is interpreted as the signature of the end of reionization at around $z \sim 6$ (Stark et al. 2010; Pentericci et al. 2014). Neutral hydrogen acts to significantly scatter Lyα, which diffuses the emission, and in the presence of dust, this causes attenuation, which makes the feature difficult to detect at $z > 6$ (Vanzella et al. 2011; Treu et al. 2013; Pentericci et al. 2014; Oesch et al. 2016; Hoag et al. 2017). Alternatives to Lyα are therefore required to obtain accurate redshift measurements of the most distant galaxies.

Interestingly, the carbon line emission may come to the rescue. This emission stems from atomic transitions that are visible both in the submillimeter domain with the [CII]-158 μm line (e.g., Carilli & Walter 2013; Capak et al. 2015; Pentericci et al. 2016; Bradač et al. 2017) and in the UV rest-frame domain with the CIII] emission at $\lambda \sim 1908$ Å, combined with the more complex CIV-λ1549 feature, which is observed both in emission from photoionization processes and in absorption (Schmidt et al. 2017). The CIII] and [CII] lines are complementary probes of the ISM and provide information on the status of the ionized and neutral gas, as outlined in simulations (e.g., Maio et al. 2016; Pallottini et al. 2017). In the UV rest-frame the HeII-λ1640 Å line is also expected to be present as a tracer of the first stellar populations such as Population III stars (PopIII), which was only present on short timescales of a few million years (e.g., Schaerer 2003; Cassata et al. 2013; Sobral et al. 2015), or of young stellar populations (Cassata et al. 2013; Kehrig et al. 2015).

The CIII]-λ1908 emission has recently been proposed as an alternative to Lyα to identify distant galaxies for which there is no Lyα in emission (Stark et al. 2014). At intermediate redshifts, CIII] emission has been reported to start with the first large spectroscopic census of LBGs (Shapley et al. 2003). At these redshifts, this line seems to be more prominent for low-mass systems, and it may be correlated to Lyα (Stark et al. 2014). Several studies report CIII] emission at $2 < z < 4$, either from individual galaxies (Erb et al. 2010; Talia et al. 2012; Karman et al. 2014; Steidel et al. 2014) or in stacks with a high signal-to-noise ratio (S/N; Shapley et al. 2003), independently of whether Lyα is in emission or not (Le Fèvre et al. 2015). At $z > 6$, CIII] is now reported in the observed spectra of several galaxies (Stark et al. 2015), but it is absent in others (Sobral et al. 2015; Schmidt et al. 2016) with solid upper limits (Shibuya et al. 2018). However, the prevalence of CIII] emitters is as yet unknown, and a robust reference to the properties of low- to intermediate-redshift analogs to the high-redshift CIII] emitters is therefore needed for this line to be useful in analyzing star-forming galaxies at the highest redshifts (Rigby et al. 2015; Du et al. 2017; Stroe et al. 2017; Amorín et al. 2017). Photoionization models indicate that CIII] emission may occur without Lyα in emission (Jaskot & Ravindranath 2016), which supports the idea that this line is useful to identify redshifts when Lyα is not present in emission.

The CIII]-λ1908 emission offers an interesting opportunity for a diagnostic of the physical conditions in distant star-forming galaxies. It is a doublet, a combination of [CIII]-λ1907 Å, which is a forbidden magnetic quadrupole transition, and CIII]-λ1909, which is a semi-forbidden electro-dipole transition (Stark et al. 2014). Its critical density is $N_e \approx 10^{10}$ cm^{-3}, and it requires an ionizing potential of 24.4 eV. In star-forming galaxies the strong ionizing flux produced by young hot stars may be sufficient to photoionize carbon with the production of CIII] photons. The strong ionizing background produced by active galactic nuclei (AGN) also leads to the ubiquitous CIII] emission that is observed in quasar spectra (Vanden Berk et al. 2001). Strong CIII] emission with an equivalent width EW(CIII]) in excess of 20 Å can mainly be produced by the hard ionizing spectrum of an AGN, or in exceptional cases, by extreme stellar populations, as described in Nakajima et al. (2018). Sufficient ionizing flux may also arise in the presence of shocks, for example, those produced by supernovae (SNe), jets from a radio source (e.g., Best et al. 2000), or from gas compression during a merger event (Bournaud et al. 2011). Characterizing the source of CIII] emission can therefore provide important clues on the star formation and the co-evolution with AGN, and in particular, on the possibility of AGN activity that quenches star formation. This mechanism has been proposed to evolve star-forming galaxies at high-z into quiescent galaxies at $z \sim 1-2$ and below (Silk & Rees 1998) (for a recent account, see, e.g., Barro et al. 2013; Dubois et al. 2013).

We here seek to characterize the prevalence and properties of CIII]-λ1908 emitters in the general star-forming galaxy population at redshifts $2 < z < 3.8$ using rest-frame UV spectra obtained from the large VIMOS Ultra Deep Survey (VUDS; Le Fèvre et al. 2015). The large sample of 3899 galaxies with the most reliable redshift measurements in VUDS, which is representative of the star-forming galaxy population at these redshifts, for the first time enables establishing the distribution and properties of the CIII] emission 10.8–12.5 Gyr back in cosmic time.

We summarize the VUDS survey properties relevant for CIII] observations in Sect. 2 and present the method for measuring the CIII] equivalent width and flux together with examples of individual CIII] emitters of different strengths. The average

spectral properties of the different CIII] populations are described in Sect. 3, including an attempt to identify the contribution from AGN. The Ly-α properties of CIII] emitters are discussed in Sect. 4. We derive the EW distribution of CIII] emitters and the CIII] emitter fraction among young star-forming galaxies in Sect. 5. We discuss the general observed properties of the CIII] emitters in Sect. 6, including their position on the plane of star formation rate (SFR) to stellar mass (SFR–$M_{\rm star}$). Evidence for AGN feedback that quenches star formation is presented in Sect. 7. A summary is provided in Sect. 8. The data presented in this paper are further analyzed in light of a wide grid of photoionization models, as discussed by Nakajima et al. (2018)

When we quote absolute quantities, we use a cosmology with $H_0 = 70\,{\rm km\,s^{-1}\,Mpc^{-1}}$, $\Omega_{0,\Lambda} = 0.7$, and $\Omega_{0,\rm m} = 0.3$. All magnitudes are given in the AB system. We use a definition of EW in which positive values indicate emission and negative values indicate absorption. All equivalent width measurements are given in the rest frame.

2. CIII]-λ1908 Å emission in VUDS

2.1. Detecting CIII] in the VUDS spectra

Spectra of ≈10 000 objects have been obtained for VUDS to study galaxy evolution in the redshift range $2 < z < 6+$. We refer to Le Fèvre et al. (2015) for a detailed description of the survey observations and for methods applied to process the data and measure key parameters, including the spectroscopic redshift $z_{\rm spec}$, and to Tasca et al. (2017) for a description of the VUDS-DR1 first data release.

The key element of this sample is that the spectroscopic targets are mainly selected based on their photometric redshifts, which satisfy $z_{\rm phot} + 1\sigma \geq 2.4$ and $i_{\rm AB} \leq 25$, with a well-defined selection of objects. The wavelength range of the final spectra is $3600 < \lambda < 9350$ Å, cumulating 14 h of integration time in each of the LRBLUE and LRRED grisms of the VIMOS spectrograph on the ESO Very Large Telescope (Le Fèvre et al. 2003), with a spectral resolution $R \sim 230$.

Standard data processing was performed using the VIPGI environment (Scodeggio et al. 2005), followed by redshift measurement using the EZ package (Garilli et al. 2010). The target selection produces a final VUDS sample that is representative of the star-forming galaxy population in the redshift range $2 < z < 6.5$, flux-selected from the rest-frame continuum UV luminosity. An important aspect of the VUDS is the wide field (large volume) that is covered. A total of $1\,{\rm deg}^2$ is covered in three fields that include the COSMOS, ECDFS, and VVDS-02h fields. This enables reducing cosmic variance in the redshift range of interest to below 10% (Moster et al. 2011). We identify galaxies with Lyα in emission and in absorption (Le Fèvre et al. 2015, e.g., Fig. 19 and 20), and the fraction of Lyα emitters with EW(Lyα) > 25 Å in the redshift range of this study is ∼11% (Cassata et al. 2015).

The instrumental setup translates into the ability to follow the CIII] line reliably from a redshift $z = 2$ up to $z \simeq 3.8$. At the spectral resolution of the observations, the CIII] λ1907–1909 doublet is not resolved, and for the remainder of this paper, we refer to the doublet as CIII]-λ1908, or CIII]. The ability to identify CIII] varies with the observed wavelength in a nonlinear way because the line will appear on top or in between the strong night-sky OH emission. This aspect is further discussed below. All other lines bluer than CIII] and redder than Lyα that are useful for spectral diagnostics can be followed for $2 < z < 3.8$. We therefore restricted the VUDS sample to the 3899 galaxies that were observed in the redshift range $2 < z < 3.8$. The spectroscopic redshift measurements extend from reliable (flags 2 and 9, ∼80% probability of being correct) to very reliable (flags 3 and 4, ∼100% probability of being correct, Le Fèvre et al. 2015).

A wide range of ancillary data is available for galaxies in VUDS, with physical parameters obtained from spectral energy distribution (SED) fitting of the multiwavelength photometric data (Tasca et al. 2015; Thomas et al. 2017), including stellar mass, SFR, dust extinction $E(B-V)$, age, or metallicity. The possible presence of obscured AGN in the sample, with an obscured view of the central engine, is not expected to strongly contribute to the overall UV continuum (e.g., Bundy et al. 2008; Assef et al. 2010; Hainline et al. 2012). The physical properties of galaxies derived from SED-fitting using templates that do or do not include an obscured AGN component are compared in Bongiorno et al. (2012), who found little difference on stellar masses and SFR. Galaxy sizes used in this study are drawn from the measurements reported in Ribeiro et al. (2016), and we also draw on the morphology analysis of bright clumps made in Ribeiro et al. (2017).

2.2. Measurements of the CIII]-λ1908 equivalent width and flux

Line flux and EW were measured individually in each galaxy. We first measured the flux and EW of CIII] using a custom code in IDL to define the sample of CIII] emitters (following Lemaux et al. 2010). When CIII] lies in wavelength domains with moderate to strong OH sky lines, we flag galaxies for which this is the case in the following way: we raise a "sky flag" when any such OH sky line (as given in Hanuschik 2003) falls within a 17 Å bandpass that defines the CIII] line (we use bandpasses of 25 Å and 23 Å for HeII and CIV, respectively). We then iterate manually on these measurements by performing a direct line integration using the `splot` tool in IRAF to obtain the final measurements of EW and flux, after identifying the continuum under CIII] by evaluating the continuum level on each side of the line, and updating the automated measurement if necessary. We proceed in the same way to obtain measurements of CIV-λ1549, HeII-λ1640, and other lines of interest, while for Lyα, we use a similar technique, but only estimate the continuum from the red side of the line.

We estimate the median error in measuring the EW of a line as the rms uncertainty resulting from noise on the spectra as measured on each side of the line, and we typically measure $1\sigma_{\rm median}({\rm EW}) = 1.0$ Å for all lines of interest. This results in a 3σ lower limit of 3 Å on EW(CIII]), limited by the faintness of the sources as observed in low $R \simeq 230$ resolution spectra.

For 2543 galaxies the background noise at the wavelength of CIII] is not affected by sky residuals or other instrumental defects. We find that CIII] is in emission in 1763 of these galaxies, EW(CIII]) > 0, while the S/N of the CIII] line for 429 and 120 galaxies is higher than 3 and 5, respectively.

3. Average CIII] properties from stacked VUDS spectra

To analyze the CIII] emitters, we split the VUDS sample of star-forming galaxies with $2 < z < 3.8$ and $S/N > 3$ into the following subsamples:

- EW(CIII]) > 20 Å: the very strong emitters (31 galaxies)
- 10 < EW(CIII]) ≤ 20 Å: the strong emitters (109 galaxies)
- 5 < EW(CIII]) ≤ 10 Å: the medium emitters (289 galaxies)

– $0 < \mathrm{EW(CIII])} \leq 5$ Å: the weak emitters (1334 galaxies)
– SFG: A UV-rest selected representative sample of 1455 star-forming galaxies from VUDS (with the best reliability flags 3 and 4), including 951 galaxies with $2 < z < 3$ and 504 galaxies with $3 < z < 4$.

The EW(CIII]) limits of these categories follow the increase in strength of the CIII] emission, as expected from the ionizing field increase that is known to occur from stellar populations and/or AGN photoinizing sources, as discussed in Nakajima et al. (2018). The definition of these subsamples is motivated by the goal of quantifying the observed properties of each of the samples while keeping a solid statistical basis. Varying the EW limit of the various subsamples has negligible effect on the conclusions of this section.

The median EW(CIII]) for the first four categories is 27.1, 13.8, 8.0, and 3.4 Å, respectively. This compares to EW(CIII])= 2.0 ± 0.2 and 2.2 ± 0.2 Å for the whole population of UV-rest selected star forming galaxies (SFGs) at $2 < z < 3$ and $3 < z < 4$, respectively. Examples of CIII] emitters over the range of observed EW(CIII]) are presented in Figs. 1–3.

Individual spectra of CIII] emitters show a wide range of properties. We observe that CIII] emission occurs in galaxies in which Lyα is either in emission or absorption. This is further investigated in Sect. 4. The CIV-λ1549 emission indicates a substantial flux of ionizing photons with energies in excess of 47.9 eV. Depending on the spectra, a wealth of absorption and emission lines are identified. This is best seen in the stacks (see below). The most common emission lines in addition to CIII] and Lyα are CIV-λ1549 (a blend of CIV-1549 and CIV-1551, combining nebular emission and stellar absorption) and HeII-1640, and we also observe OIII]-λ1663 (a blend of the λ1661–1666 doublet at the resolution of VUDS), NIII-λ1750, and NIV-λ1485, as well as NV-λ1240, SiII-λ1309, SiIII-λ1888, and SiIV-λ1403. In rare cases, Lyβ and OVI-λ1035 are also observed in emission.

Similarly to Le Fèvre et al. (2015), we produce summed ("stacked") spectra of VUDS galaxies in the rest-frame using the VUDS catalog redshift (as described in the presentation of the first VUDS data release, Tasca et al. 2017). These stacks are produced by normalizing the continuum between 1300 and 1600 Å and summing the flux from all galaxies in a given category defined above, using the `scombine` task under IRAF, with sigma clipping set at 3σ. In these stacks, we do not use objects that are identified as AGN, either with broad-line or NV-λ1240 emission, as presented in Sect. 6.4.

We find that the lower EW measurements include significant contamination from noise, which we correct for to obtain the fraction of emitters as a function of EW(CIII]), as described in Sect. 5. Spectra for each of the stacks are therefore selected from the complete VUDS sample galaxies, but keeping only objects whose CIII] S/N is higher than 5 and that satisfy a visual inspection such that CIII] is clear of sky-subtraction residuals or other spectral defects. A total of 43, 31, 30, and 16 spectra are stacked for the weak, medium, strong, and very strong emitters, respectively. Stacked spectra for these different categories are shown in Fig. 4. For the SFG sample we do not apply any S/N restriction because the sample is large enough to produce a stable stack.

The spectra show interesting features that change when the EW(CIII]) increases: in addition to the Lyα properties discussed in Sect. 4, we find emission lines of several atomic species, which appear and grow stronger. For the whole SFG population we observe both CIII] and HeII-λ1640 in emission, as well as a fainter CIV-λ1549 emission that is partially suppressed by strong absorption with a P-Cygni profile. It is expected to observe both CIII] and HeII in emission because these two lines are ionized under similar conditions: the energy required to ionize helium is only slightly greater than the energy required to doubly ionize carbon (24.6 vs. 24.4 eV), and faint HeII emission is frequently observed in the general population. The HeII emission presents a useful diagnostic for very young as well as more exotic stellar populations (Schaerer 2003; Cassata et al. 2013), and it will be discussed in a forthcoming paper.

As the EW(CIII]) increases, we observe in the stacked spectra that HeII and CIV become stronger, interstellar medium lines such as SiII-λ1260, OI+SiII-λ1303, CII-λ1334, and SiV-$\lambda\lambda$1393.76–1402.8 fill in, OIII-λ1663 appears for $5 < \mathrm{EW(CIII])} < 10$, and NIV-$\lambda$1645 and NIII-$\lambda$1750 are both visible for the $10 < \mathrm{EW(CIII])} < 20$ stack. The combined spectrum of the strongest emitters with $\mathrm{EW(CIII])} \geq 20$ strikingly shows a wealth of strong emission lines, as presented in Fig. 5. In addition to CIII], we identify the following lines in emission: NV-λ1240, SiII-λ1309, SiIV-λ1403, NIV]-λ1485, CIV-λ1549, HeII-λ1640, [OIII]-λ1663, NIII]-λ1750, and SiIII]-λ1888, with a spectrum comparable to that of the UV-selected AGN sample at $z \sim 2-3$ from Hainline et al. (2011). The lines OIII-λ1663, SiIII, NIII, NIV, and NV require energy levels above 35.1, 16.3, 29.6, 47.5, and 77.5 eV, respectively. This therefore agrees with observation that the ionizing field in these galaxies becomes stronger.

We provide measurements of EW and line flux relative to CIII] from the stacked spectra of the different CIII] populations in Tables A.1 and A.2 we list them for the whole SFG populations at $2 < z < 3$ and $3 < z < 4$. We also indicate the slope β of the UV continuum, parameterized as $F_\lambda \propto \lambda^\beta$, measured from the continuum values between 1400 Å and 2100 Å rest-frame (Hathi et al. 2016). To measure these continuum values, we fit the observed continuum with a cubic spline excluding 30 Å around known emission and absorption features. We observe that β is smaller (the continuum steeply declines with wavelength) for the strongest CIII] emitters with $\beta = -1.76 \pm 0.06$, and it gradually becomes flatter for populations with decreasing EW(CIII]). It reaches $\beta = -0.92$ for the whole SFG population. This observation corroborates that a stronger UV ionizing field is present for the strongest CIII] emitters.

4. Lyman-α properties of CIII] emitters

We investigate the relationship between CIII] and Lyα emission in Fig. 6 using the sample of CIII] emitters with $S/N > 5$. The relation between CIII] and Lyα from the spectral stacks (Table A.1) shows a strong correlation with a Pearson correlation coefficient $r_\mathrm{P} = 0.99$ and Spearman rank correlation coefficient $r_\mathrm{S} = 1$ (r_P or r_S equal to one indicate a perfect one-to-one correlation). However, from the individual emitters, while we observe a trend for the strongest CIII] emitters to be strong Lyα emitters (LAE) as well, with a correlation significant at about the 3σ level (Student t-test), this correlation has a large dispersion. This correlation further weakens when we restrict the sample of CIII] emitters to $\mathrm{EW(Ly}\alpha) < 50$ Å with $r_\mathrm{P} = 0.2$, which is similar to the EW reported by Rigby et al. (2015). The analysis of individual emitters demonstrates that Lyα in emission increases the probability of detecting CIII], but it also shows that strong Lyα emission does not necessarily mean strong CIII] emission, or vice versa. There are indeed numerous examples of galaxies with CIII] in emission and no or weak Lyα emission (some are presented in Figs. 1 and 3). We reach similar conclusions based on the CIV-λ1549 line vs. Lyα emission.

This behavior is somewhat expected as the radiative transfer of Lyα or CIII] photons is markedly different. As a striking

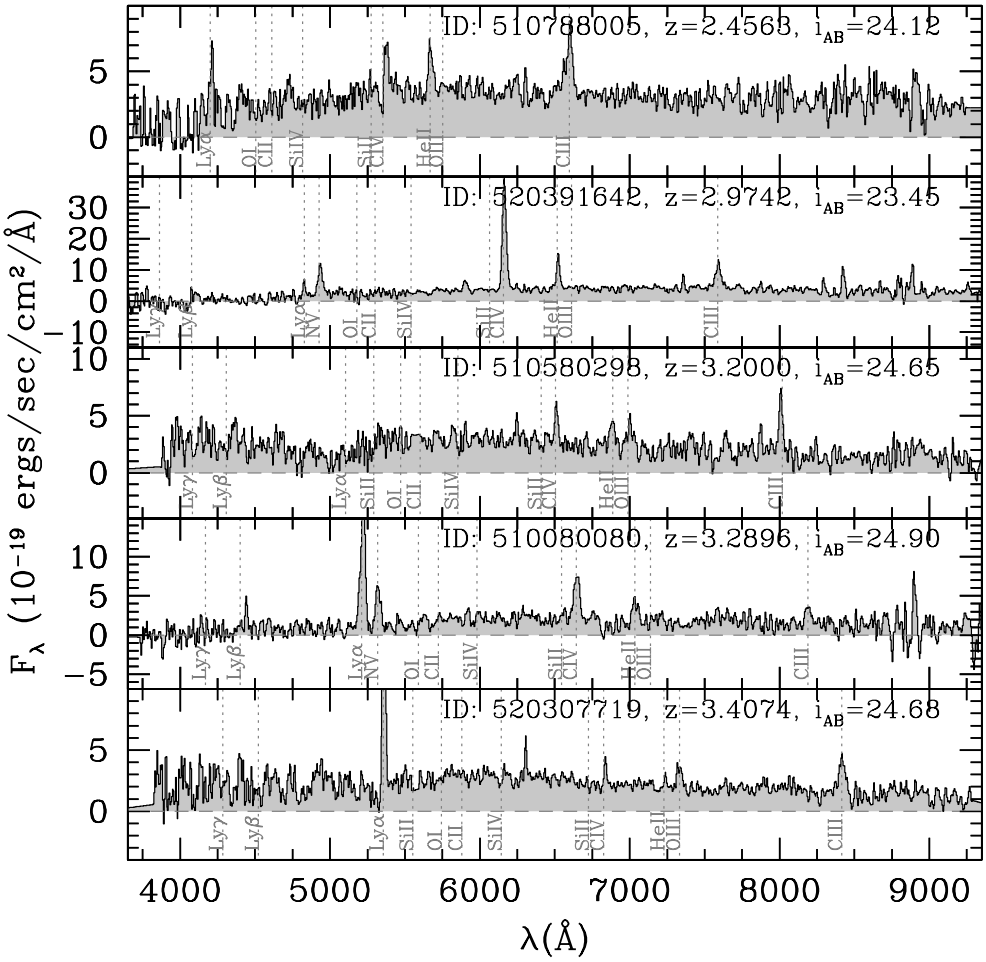

Fig. 1. Example VUDS spectra of CIII]1908 emitters with very strong EW(CIII]) ≥ 20 Å. The spectra of strong CIII] emitters are highly divers: they include strong Ly-α emission as well as weak Ly-α emission (ID:510788005 and ID:510580298).

example we point to object 520391642 (second from the top in Fig. 1), which shows strong CIII] (EW > 20), as well as CIV, HeII, or NV, but only weak Lyα emission. Our results compare well with the literature when the large spread of the relation between EW(CIII]) and EW(Lyα), the selection, and the size of different samples is taken into account. The average properties from stacks show that our results agree well with those of Shapley et al. (2003). VUDS galaxies span a broad range of properties, including galaxies with and without Lyα in emission, expanding from smaller and possibly biased samples for which a stronger correlation between Lyα and CIII] is reported (Stark et al. 2014, 2015; Rigby et al. 2015; Guaita et al. 2017).

We find that the chance of emitting CIII] and CIV at an appreciable level (EW > 3 Å) for galaxies with EW(Lyα) > 25 (the broadly used definition of a LAE) is 42% and 20%, respectively. For galaxies that emit both Lyα and CIII] at these levels, the median EW(CIII]) is 7.7 Å, compared to a median EW(CIV) of 3.4 Å for the average LAE emitting CIV.

The overall weak correlation that is observed between CIII] and Lyα emission strength for individual galaxies is in line with findings from photoionization models (e.g., Jaskot & Ravindranath 2016; Zackrisson et al. 2017; Nakajima et al. 2018) when a broad range of conditions such as ionizing fields, geometry, and dust opacity is taken into account.

5. Distribution of EW(CIII])

To answer the question of how frequently CIII] emission is observed in UV-selected galaxies, we seek to establish the fraction of CIII] emitters in the VUDS sample as a function of EW(CIII]). While it is straightforward to identify strong CIII] emitters, it is more difficult to separate weak emitters from noise. We therefore proceed with a statistical analysis of the distribution of CIII] emission for the 3899 VUDS galaxies with $2 < z < 3.8$.

If CIII] emission is absent and in the presence of noise, the line measurement resulting from the process presented in Sect. 2.2 could result in either a false-positive or negative EW. As CIII] is only expected in emission, we use the distribution of EW measurements that indicates absorption as an estimate of how many CIII] emission lines could be produced from noise spikes, under the assumption of a Gaussian noise distribution. We compute the distribution for EW(CIII]) < 0, derive the EW of this distribution positive (emission), and subtract this distribution from the distribution of EW(CIII]) > 0 to statistically correct the distribution of EW(CIII]) for false CIII] emission measurements and obtain the EW distribution for CIII] emitters. For each EW bin we compute the associated error from the quadratic sum of the observed numbers of emitters and non-emitters.

The resulting rest-frame EW(CIII]) distribution is shown in Fig. 7, where it is presented as the fraction of emitters with a given EW(CIII]) over the full population of UV-selected star-forming galaxies, both differential and cumulative. The fraction of emitters decreases from a peak at low EW down to the largest narrow-line emission galaxies with EW(CIII]) ∼ 40 Å, as expected. We find that the population of star-forming galaxies contains 4.0 ± 1.2% of strong emitters with EW(CIII]) > 10 Å, including 1.2±0.4% of very strong CIII]

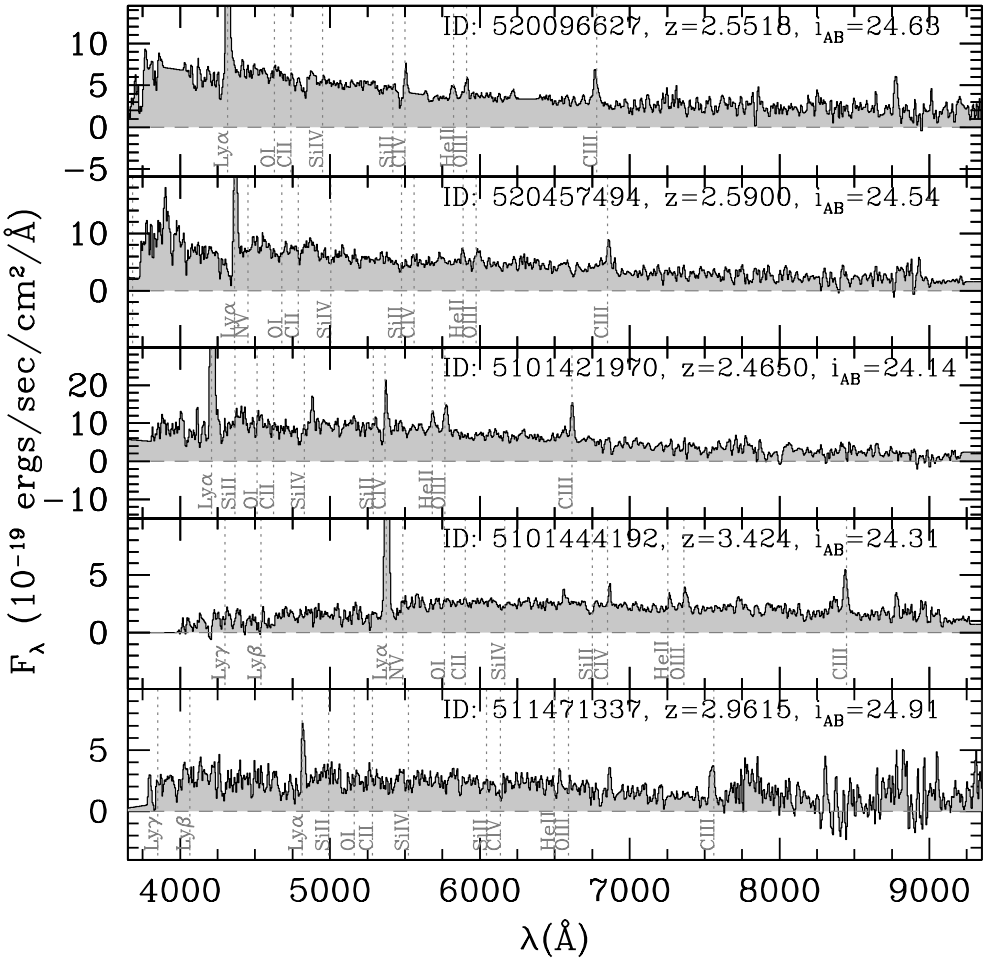

Fig. 2. Example VUDS spectra of strong CIII]1908 emitters with $10 < \mathrm{EW(CIII])} < 20$ Å.

emitters with EW(CIII]) > 20 Å, and 20 ± 3.1% of weak emitters 3 < EW(CIII]) < 10 Å. The line emission distribution shows that CIII] emission is present above EW(CIII]) = 3 Å for less than one-fourth of UV star-forming galaxies at $z \sim 3$.

In addition to Lyα, the CIII] line remains the most frequent emission line observed at EW > 3 Å. By comparison, a similar analysis shows that about 10% of the galaxies emit CIV at a level EW(CIV) > 3 Å that is sufficient to claim detection from VUDS spectra.

6. Properties of CIII] emitters

6.1. L_{NUV}, M_{star}, SFR, morphology, of CIII] emitters

In this section we compare the population of CIII] emitters to the general properties of the star-forming galaxy population. We present the relation between the rest-frame near-UV luminosity L_{NUV}, the SFR, M_{star}, SSFR, and total size r_{tot} as a function of EW(CIII]) in Fig. 8, including the significance of the correlation using the Pearson correlation coefficient r_{P} and Student t-test significance.

We find that the L_{NUV} luminosity decreases with increasing EW(CIII]), from a median $L_{\mathrm{NUV}} = 10.2$ in $5 < \mathrm{EW(CIII])} < 20$ to $L_{\mathrm{NUV}} = 9.9$ for EW(CIII]) ≥ 20, with $r_{\mathrm{P}} = -0.28$, a correlation that is significant at the 3.4σ level. If this trend is maintained to higher redshifts, we may expect to observe a higher fraction of CIII] emitters in lower luminosity galaxies into the reionization epoch than was reported in Sect. 5.

The SFR also decreases with increasing EW(CIII]) ($r_{\mathrm{P}} = 0.3$, significant at 3.6σ), with a decrease of ∼20% for emitters with EW(CIII]) ≥ 20 compared to $5 < \mathrm{EW(CIII])} < 20$. With EW(CIII]) dependent on the ionizing field, and the strongest CIII] emitters partially powered by AGN (Nakajima et al. 2018), this relation may be due to star formation quenching. This is discussed in Sect. 6.3.

The strongest CIII] emitters have a weak trend of higher stellar masses than the weaker emitters, but this is not significant ($r_{\mathrm{P}} = 0.08$, 0.6σ). The trend in SFR and M_{star} combines for a weak dependency of SSFR on EW(CIII]) ($r_{\mathrm{P}} = -0.31$, 3.3σ). There is no apparent trend with EW(CIII]) of the dust extinction from the $E(B-V)$ computed from SED fitting.

A visual morphological classification is performed on each of the CIII] samples (Table 1), using the HST F814W images available in the COSMOS and ECDFS fields (for details on the imaging data on the VUDS sample, see Ribeiro et al. 2016). The morphology of very strong CIII] emitters is dominated by compact galaxies ($r_{100} < 1$ kpc, see Ribeiro et al. 2016) and galaxy pairs with a separation smaller than 20 kpc (see Ribeiro et al. 2017). The population of strong CIII] emitters shows a high fraction of compact galaxies, with an equal fraction of pairs. This is comparable to the strong emitters within the error bars. For the medium and weak emitters, the fraction of compact galaxies is low, the pair fraction remains similar to the other CIII] samples, but clumpy galaxies dominate, together with extended and symmetric galaxies. It therefore appears that CIII] is preferentially emitted in compact and interacting systems, as has been pointed out in the smaller VUDS subsample of Amorín et al. (2017). This is further supported by the distribution of sizes as a function of EW(CIII]) presented in Fig. 8. The sizes clearly decrease

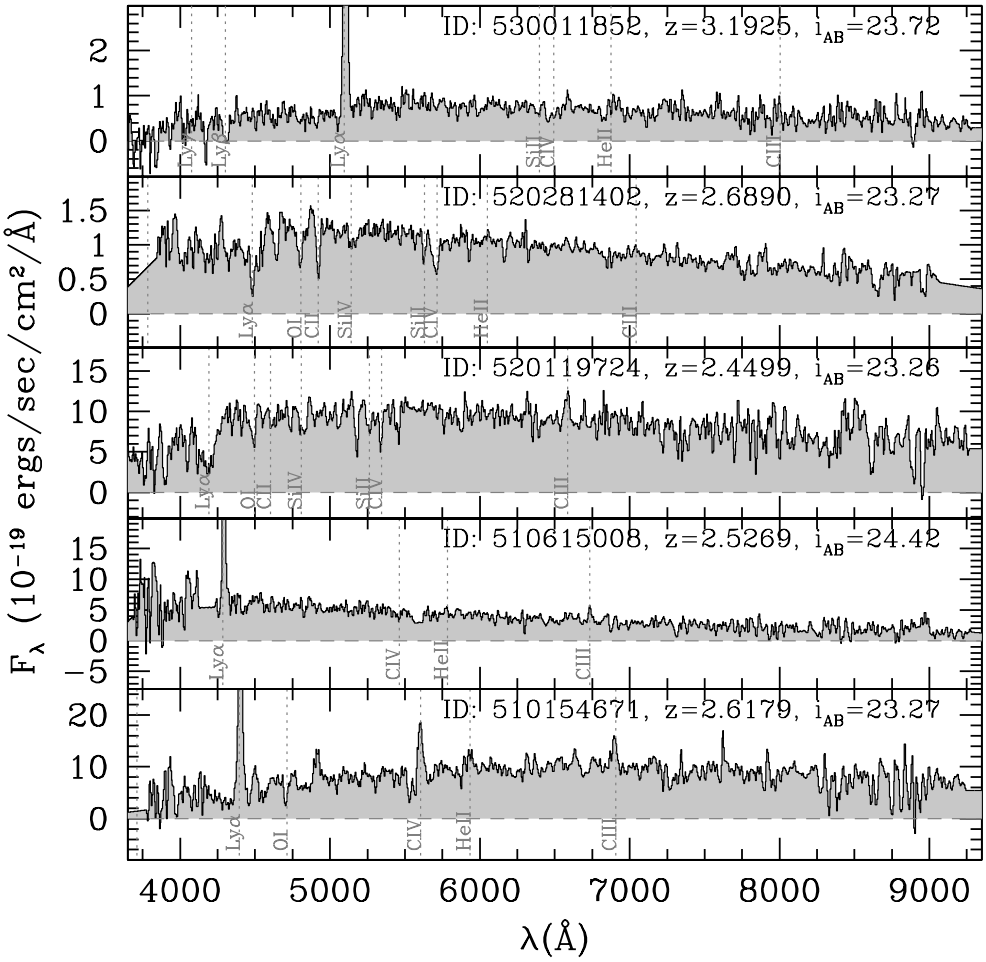

Fig. 3. Example VUDS spectra of weak CIII]1908 emitters with $0 < \mathrm{EW(CIII])} < 5$ Å.

with increasing EW(CIII]) (with $r_P = -0.44$, which correlation is significant at the 5.5σ level).

6.2. Outflow velocities

The velocity of ISM lines compared to the systemic velocity is presented in Fig. 9 as measured from the stacked CIII] spectra, and the median velocity derived from the individual line measurements is presented in Fig. 10. We set the systemic velocity on the CIII] line, and verified that this agrees with photospheric absorption lines CIII]-λ1176 and SV-λ1501, as well as with HeII-λ1640 emission (see Talia et al. 2017). To measure the velocity of the ISM, we used the ISM absorption lines in Table 2 of Talia et al. (2017), except for the FeII-λ1608 line, which was measured to be compatible with being at rest and may be contaminated by a blend of absorption features (FeIII, AlIII, and NII), as pointed out by Talia et al. (2017). We also excluded the CIV-λ1549 line, which is a combination of emission and absorption. For the whole SFG population at $2 < z < 3$ and $3 < z < 4$ and the CIII] emitters with $5 < \mathrm{EW(CIII])} < 10$ Å, we detected and used these lines to compute the median velocity difference $\Delta V = \delta\lambda/\lambda \times c$. For $5 < \mathrm{EW(CIII])} < 10$ Å emitters we did not use SiV-λ1402.77 and AlIII-λ1854.72,1862.79 because they are only weakly detected. For $\mathrm{EW(CIII])} > 20$ we used SiII-λ1260, SiIV-λ1393.76,1402.77, SiII-λ1526.71, and AlIII-λ1854.72,1862.79; the other lines are not detected in the stack of this smaller sample. At the spectral resolution used for the VUDS sample (Sect. 2), the instrumental resolution is ~1000 km s^{-1}, allowing for an accuracy in relative velocity measurements of ~250 km s^{-1} (Le Fèvre et al. 2015), and when all ISM lines are well detected as in the whole SFG samples at $2 < z < 3$ and $3 < z < 4$, the velocity dispersion of the line velocity measurements is $\sigma_V(\mathrm{ISM}) \sim 40{-}50$ km s^{-1}.

The resulting relative velocity measurements are quite striking (Fig. 10): we find low-velocity outflows with 50–150 km s^{-1} for the whole SFG populations at $2 < z < 3$ and $3 < z < 4$ and medium CIII] emitters, while the outflow velocity increases to 445 ± 110 km s^{-1} for the strong $10 < \mathrm{EW(CIII])} < 20$ emitters, and reaches 1014 ± 205 km s^{-1} for the very strong emitters with $\mathrm{EW(CIII])} > 20$, which is well beyond the escape velocity of these galaxies (Cimatti et al. 2013) and is comparable to what is observed in SFGs with AGN at $z \sim 1{-}2$ (e.g., Genzel et al. 2014). As star formation does not seem to be capable to produce outflow velocities beyond ~600 km s^{-1} even for strong starbursts with maximally efficient winds (Thacker et al. 2006), we conclude that the outflows reported here for the stronger CIII] emitters are produced by an AGN. This is further discussed in the following sections.

6.3. CIII] emitters in the SFR vs. M_{star} plane

The position of CIII] emitters with respect to the main sequence (MS) of star-forming galaxies in the stellar mass vs. SFR plane is presented in Fig. 11. The strong and very strong emitters show a trend of being located below the MS that is observed in the same redshift range (Tasca et al. 2015). This is particularly evident for the very strong emitters with $\mathrm{EW(CIII])} > 20$, which are mostly below the MS. For this population it is quite striking

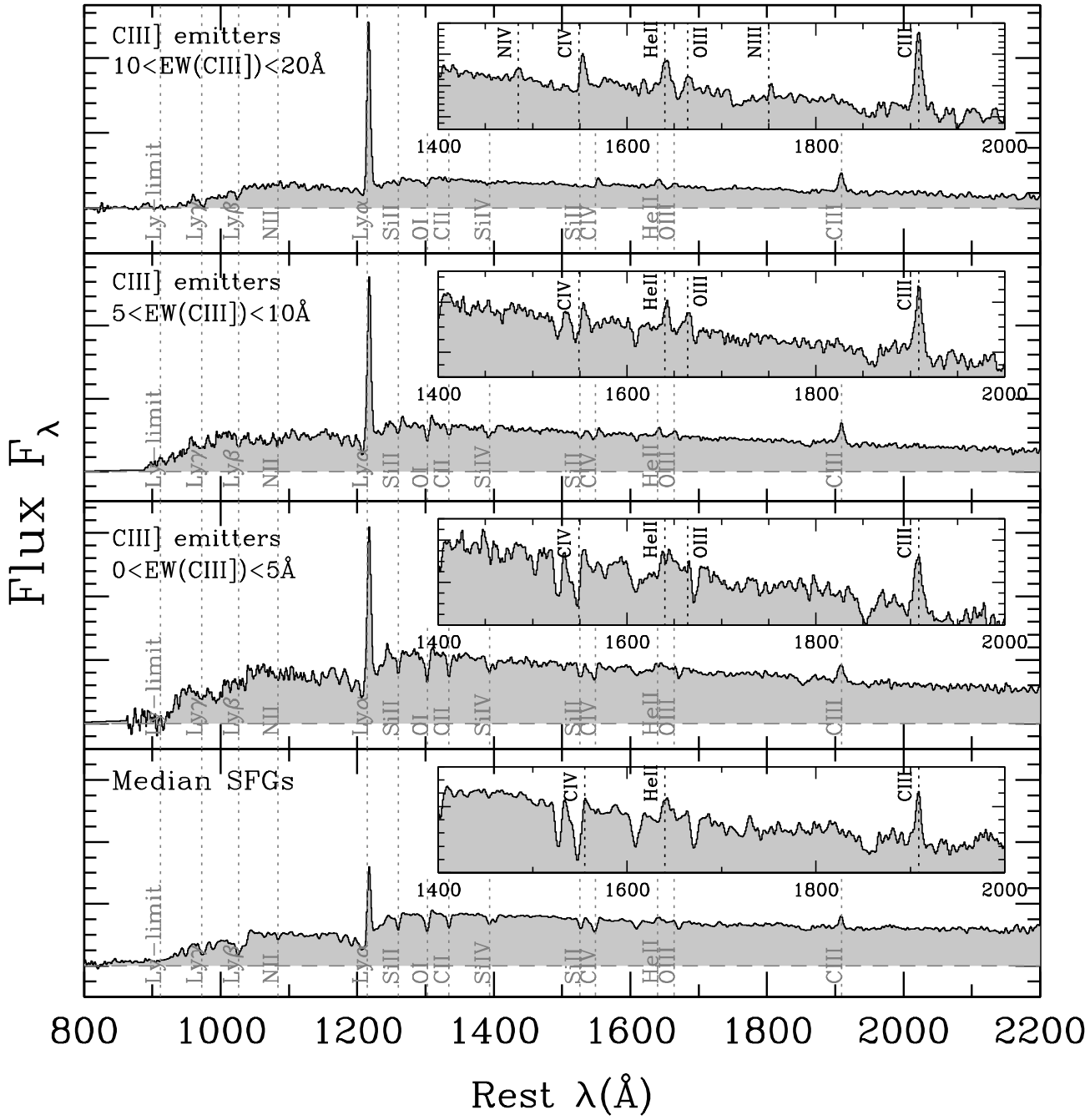

Fig. 4. Composite spectra of CIII]1908 emitters identified in the VUDS survey at $2 < z < 3.8$. *From top to bottom*: stack of 43 emitters with $10 < \mathrm{EW(CIII])} < 20$, 31 emitters with $5 < \mathrm{EW(CIII])} < 10$, 30 emitters with $0 < \mathrm{EW(CIII])} < 5$, and for comparison, a stack of 450 galaxies that are representative of the general SFG population in the redshift range $2.8 < z < 3.8$.

to observe galaxies with low or even very low SFR, but with very strong CIII] emission. In Fig. 12 we present the distribution of the difference between the SFR of galaxies and the MS identified in Fig. 11. The mean SFR difference increases from $d_{\mathrm{MS}}(\mathrm{SFR}) = +0.14 \pm 0.03$ (dex, above the MS) for emitters with $0 < \mathrm{EW(CIII])} < 10$ Å, to $d_{\mathrm{MS}}(\mathrm{SFR}) = -0.10 \pm 0.08$ for $10 < \mathrm{EW(CIII])} < 20$ Å, to $d_{\mathrm{MS}}(\mathrm{SFR}) = -0.27 \pm 0.07$ (below the MS) for $\mathrm{EW(CIII])} > 20$ Å. The total shift in SFR of $d_{\mathrm{MS}}(\mathrm{SFR}) = -0.41$ dex between the weak CIII] emitters and the very strong emitters is significant at more than a 5σ level.

The star formation of the weaker CIII] emitters appears to be higher than for the bulk of the SFGs. While the whole SFG population has a median $\mathrm{EW(CIII])} \sim 2$ Å (Table A.1), the population of weak and medium emitters has $\mathrm{EW(CIII])} = 3.4$ Å and 8.0 Å, respectively. Producing $3 < \mathrm{EW(CIII])} < 10$ Å in the absence of an AGN requires enhanced star formation, which is consistent with this population being above the MS (Nakajima et al. 2018).

The distance to the MS of the strong and very strong CIII] emitters is more puzzling because the distance to the MS of these populations is increasingly below the MS, with a SFR of about half that on the MS. A possible interpretation is that the star formation for a fraction of the strong emitters and a majority of the very strong emitters is subject to quenching of star formation. Some of the very strong emitters are more than a factor of 10 below the MS, which means that the quenching must be very effective, while at the same time, they maintain a very strong

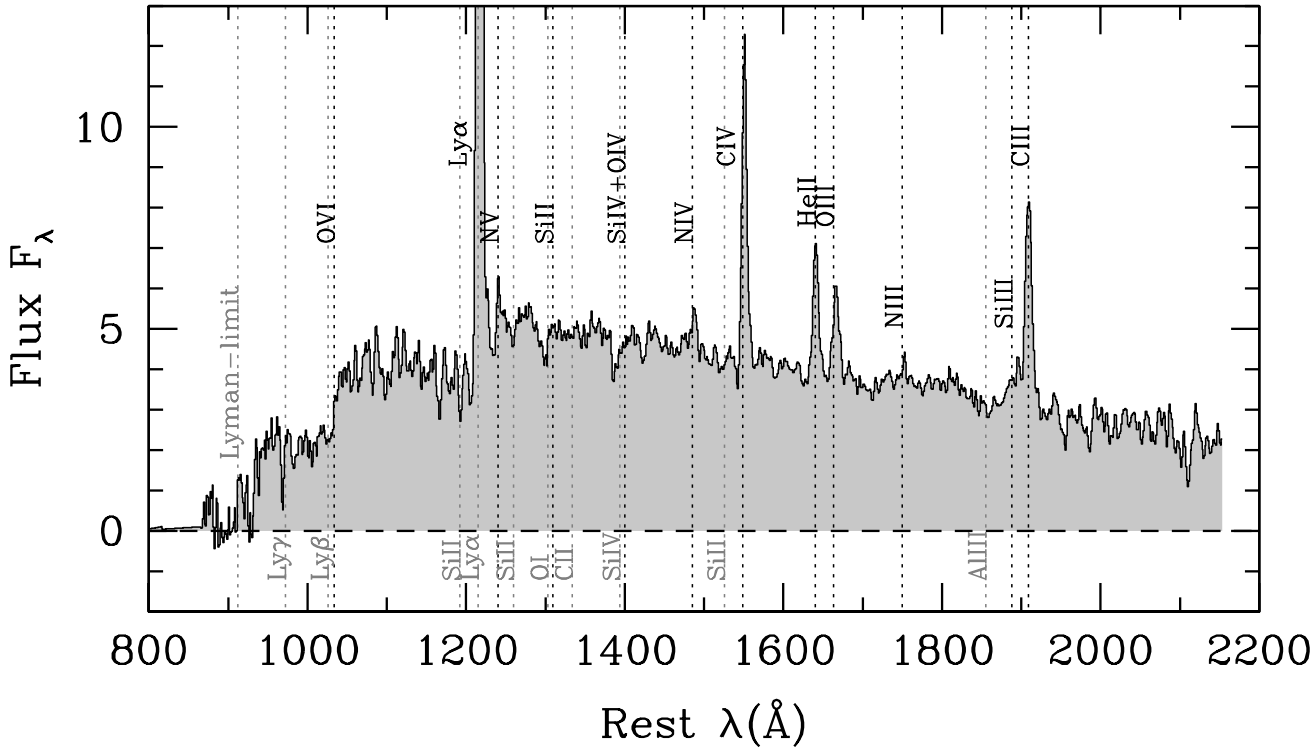

Fig. 5. Composite spectrum of 16 CIII]-λ1908 emitters identified in the VUDS survey at $2 < z < 3.8$, where CIII] is detected in emission with $S/N > 5$ and EW(CIII]) > 20 Å. The main emission lines associated with CIII]-λ1908 emission can be identified as Lyα, NV-λ1240, NIV]-λ1485, CIV-λ1549, HeII-λ1640, OIII]-λ1663, NIII]-λ1750, and SiIII]-λ1888.

ionizing field that is required to produce EW(CIII]) in excess of 20 Å.

We further investigate the properties of the CIII] emitters by considering the age distribution of the different categories, as presented in Fig. 13, with ages computed in Thomas et al. (2017) from the joint fitting of VUDS spectra and rest-UV and optical photometry. We use as an age definition the time since the onset of the last star formation event, which dominates the star formation history, as modeled by a delayed exponential (see Thomas et al. 2017). The median age of the galaxies is about the same for the weak and medium emitters, with 0.29 ± 0.07 and 0.30 ± 0.05 Gyr, respectively, it increases to 0.46 ± 0.09 Gyr for the strong emitters and reaches up to 0.82 ± 0.13 Gyr for the very strong emitters. This relative age difference does not qualitatively change when we use other age definitions such as the mass-weighted age. This may indicate that the strongest emitters have been subject to star-formation quenching for a longer time, as discussed in Sect. 7.

As pointed out in Sect. 2, AGN might not dominate the age-sensitive regions of the SED, therefore the presence of AGN is not expected to significantly alter the stellar mass or SFR measurements obtained from SED fitting (see, e.g., Bongiorno et al. 2012), and the results presented here are thus qualitatively expected to hold. However, more sophisticated SED modeling will be in order when data with higher S/N will become available so that AGN can be separated from stellar populations.

6.4. Type I and Type II AGN in the sample of CIII] emitters

We make an attempt to identify the contribution of AGN to the SFG population based on standard line diagnostic criteria. Four objects among the 3899 sources with $2 < z < 3.8$ meet the conditions to be classified as broad-line type I AGN when we impose that one or more of the observed emission lines in the VUDS spectral window have an $FWHM > 1000\,\mathrm{km\,s^{-2}}$. The spectra of these objects are similar to broad-line quasar spectra at similar redshifts (e.g., Vanden Berk et al. 2001), as can be seen in the stacked spectrum in the bottom panel of Fig. 14.

The NV-λ1240 emission requires a strong ionizing field ~77 eV, and therefore has been proposed as a criterion to identify narrow-line type II AGN (e.g., Hainline et al. 2011). As this criterion may not strictly exclude other ionization source for weak NV emission, we searched for emitters with EW(NV) > 10 Å, which are most likely type II AGN, and we identified seven such narrow emission line objects.

The stacked spectrum of the strong NV emitters is shown in the top panel of Fig. 14. We easily identify Lyβ, OVI-λ1032, Lyα, NV-λ1240, SiIV-λ1403, NIV-λ1485, CIV-λ1549, HeII-λ1640, OIII]-λ1664, CIII]-λ1908, CII]-λ2326, and [NeIV]-λ2424 in emission. The CIV/CIII] flux ratio for these VUDS narrow-line AGN ranges from 1.2 to 4.7 with a median CIV/CIII] = 2.7. This ratio is lower than the class A composite spectrum of type II quasars presented in Alexandroff et al. (2013) with CIV/CIII] = 7.5. However, it is higher than the sample of type II AGN in Hainline et al. (2011), for which CIV/CIII] ~ 1.3, rather consistent with that of radio galaxies at similar redshifts (Villar-Martin et al. 1997; Stern et al. 1999; Matsuoka et al. 2009), is higher than SFGs, which have a typical ratio below unity (Nakajima et al. 2018).

Some contribution to the CIV-λ1549, SiIV-λ1403 and NV-λ1240 may be coming from stellar winds that are produced by strong star formation. Studying a sample of local analogs to high-z Lyman-break galaxies, Heckman et al. (2011) indicated that a broad NV-λ1240 line, with a P-cygni profile, could arise from stellar winds that are produced by hot (O) stars. Still, only a few galaxies have CIV/CIII values that are comparable to even

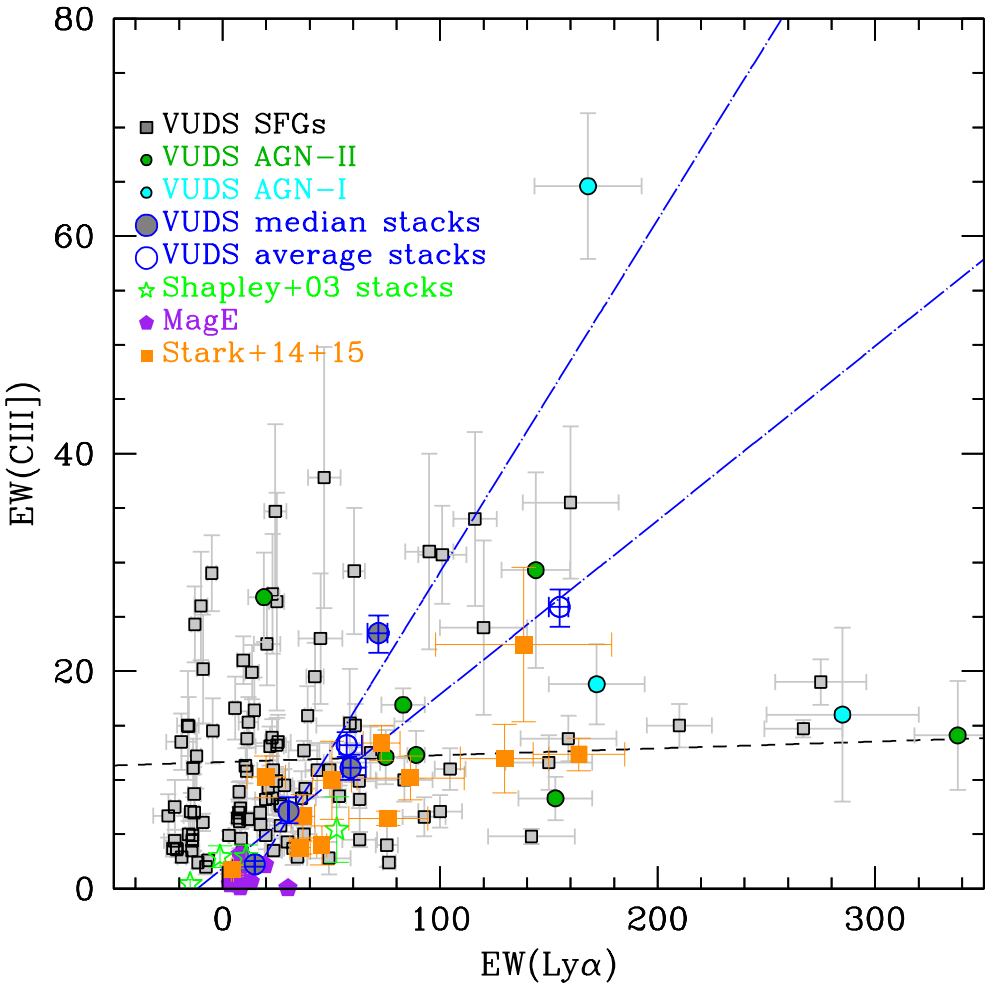

Fig. 6. Rest-frame equivalent width of CIII]-λ1908 EW(CIII]) as a function of EW(Lyα). The least-squares fit to the individual data points (black squares) is represented by the black dashed line. The individual galaxies show only a weak correlation that is significant at about the 3σ level, with a large dispersion. Galaxies with strong Lyα and weak CIII] are observed, as well as galaxies with strong CIII] and Lyα in absorption. The EW(CIII]) vs. EW(Lyα) points for the median-stacked spectra of the different categories defined in Sect. 3 are indicated as blue circles filled with gray, while values for the average stacks in Table A.1 are indicated as open blue circles. The correlation between EW(CIII]) and EW(Lyα) appears to be very strong (r_P = 0.99, r_S = 1) and hides the wide range of properties of CIII] vs. Lyα. As a comparison with the literature, we plot the observed values from the different Lyα samples of Shapley et al. (2003) (green stars, average for Lyα samples), Rigby et al. (2015) (purple diamonds), and Stark et al. (2014, 2015) (orange squares).

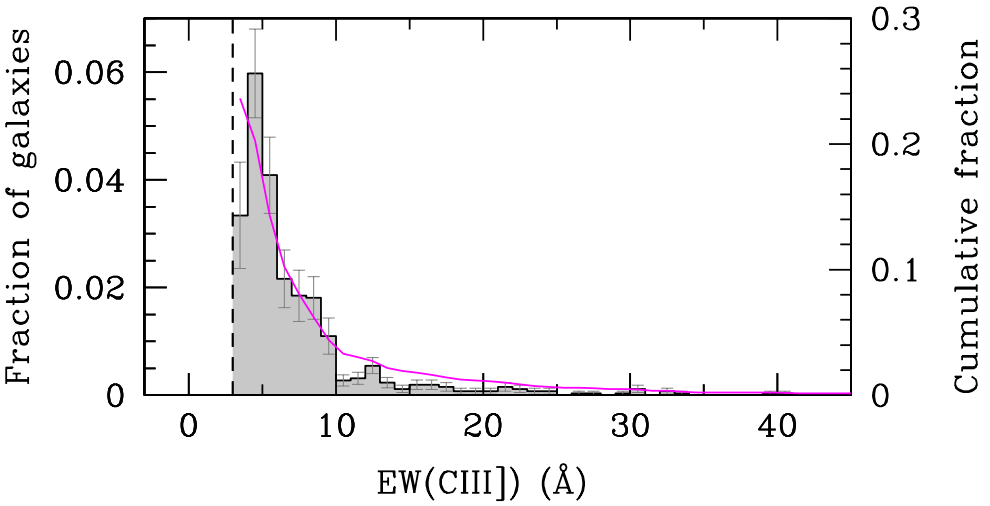

Fig. 7. Distribution of CIII]-λ1908 equivalent width EW(CIII]) in the UV-selected star-forming population at 2 < z < 3.8. The shaded histogram shows the fraction of galaxies with a given EW(CIII]) in bins of δEW = 1 Å (left Y-axis), with Poisson uncertainties from the population statistics indicated as error bars. The cumulative fraction of galaxies with EW(CIII]) above a given EW(CIII]) limit is drawn as the continuous magenta line (values on the right Y-axis), relative to the total population of SFGs at that redshift. About 24% of SFGs with 2 < z < 3.8 present CIII]-λ1908 Å emission with EW(CIII]) ≥ 3 Å.

the lowest values in NV-detected galaxies, which means that a pure star formation interpretation is probably not correct at these low redshifts.,nterestingly, two out of seven strong NV emitters show weak or absent Lyα emission (see object 520391642 in Fig. 1). These two objects present a red UV continuum (β slope +2.3 and +0.8) and may therefore have dusty ISM conditions that prevent Lyα from escaping. The AGN type II stack has a much redder continuum slope β = +0.2 ± 0.05 than the CIII]-selected star-forming populations discussed in Sect. 3 with β > −1.6. These results are in line with those presented by Hainline et al. (2011). This indicates that the internal extinction is stronger in the AGN population, and that a combination of a dust-obscured AGN and star formation component may produce the observed spectra.

We note that the AGN sample we have identified here based on NV are almost certainly as we show below, a small subset of the total AGN population. The criteria for identifying type II AGN from UV-rest spectra vary from sample to sample in the literature, and we point out that a quantitative spectral line analysis is required, rather than an empirical

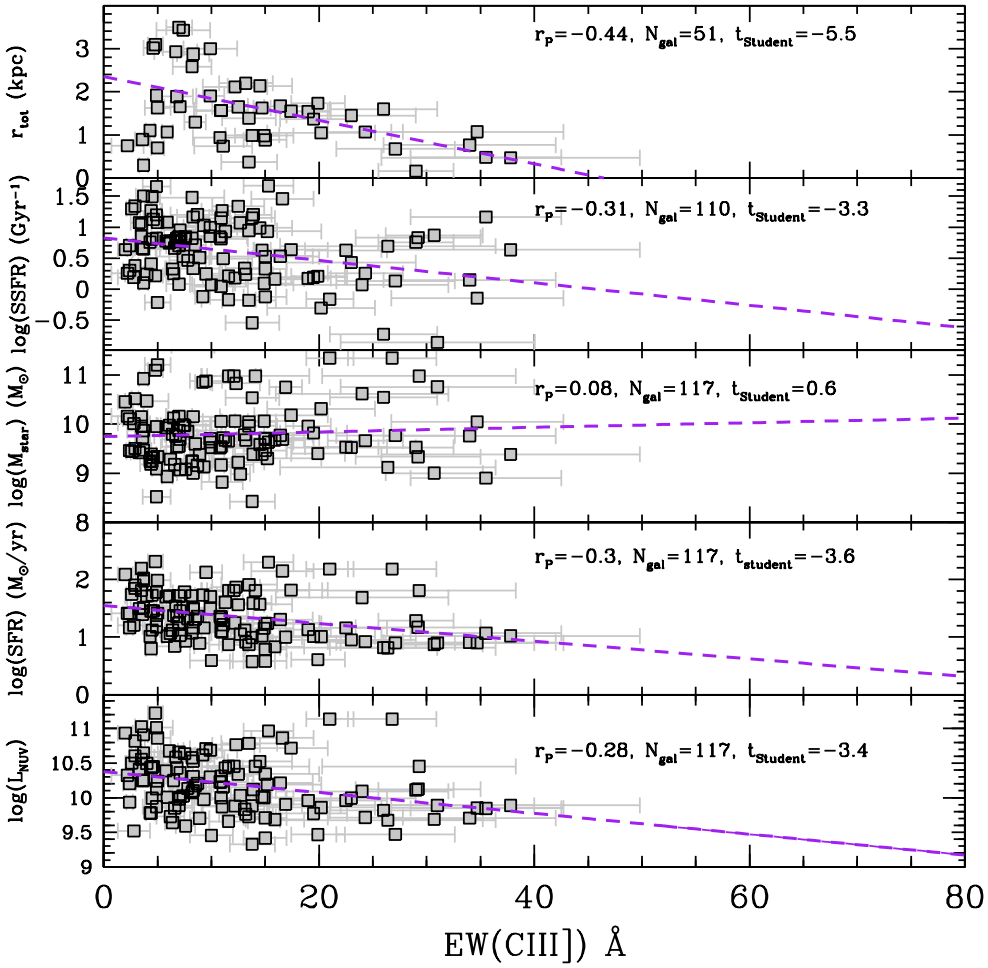

Fig. 8. Properties of CIII] emitters, *from bottom to top*: $L_{\rm NUV}$, SFR, $M_{\rm star}$, SSFR, and total size properties of CIII] emitters as a function of EW(CIII]). A least-squares fit to the data is shown as the purple dashed lines, and the Pearson correlation coefficient $r_{\rm P}$, number of objects, and the significance of the correlation (Student t-test) are indicated in the upper right corner of each panel. The $r_{\rm tot}$ measurements are limited to the COSMOS and ECDFS fields for which HST imaging is available (Ribeiro et al. 2016).

Table 1. Visual classification of the CIII] emitter morphology.

Sample	Compact $r_{\rm T} < 1$ kpc [(1)]	Pairs $r_{\rm P} < 20$ kpc [(2)]	Clumpy and extended
0 < EW(CIII]) < 10 Å	6 ± 0.6%	40 ± 1.5%	54 ± 1.8%
10 < EW(CIII]) < 20 Å	39 ± 6%	39 ± 6%	22 ± 4%
EW(CIII]) > 20 Å	25 ± 9%	44 ± 11%	31 ± 10%

Notes. [(1)]Total radius (Ribeiro et al. 2016). [(2)]Transverse pair separation.

classification. This is developed in Nakajima et al. (2018), who discussed various diagnostic diagrams using UV emission lines. The diagrams were based on photoionization models, and in particular indicated that different line ratios are requirede to separate star formation from AGN. Nakajima et al. (2018) cdlaim that the population of strong and very strong CIII] emitters presented here must include AGN to explain the high EW(CIII]) and the location of these galaxies in diagnostic diagrams that are assembled from observed UV line ratios. This is further discussed in Sects. 6 and 7.

We searched for individual X-ray counterparts of CIII] emitters using *Chandra* observations in the CDFS (the 7 Ms catalog of Luo et al. 2017), in COSMOS (the legacy catalog of Civano et al. 2016; Marchesi et al. 2016), and the XMM data in the VVDS-02h field (the XMM-LSS catalog of Chiappetti et al. 2013), with flux limits $L_{\rm X}$(2–10 keV) ranging from 3×10^{42} to 3×10^{44} erg s^{-1} at $z \sim 3$. We found a total of eight X-ray counterparts, one in CDFS (id 530029221), six in COSMOS (ids 510080080, 510788005, 511707398, 510793659, 510164473, and 5121237451), and one in the VVDS-02h (id 520426550) (see also Talia et al. 2017). The X-ray luminosity of these sources have is in the range $43.8 < \log(L_{\rm X}(2\text{–}10\,{\rm keV}) < 44.5$. All of these objects are identified as AGN following the NV analysis described above, except for one (id 510788005), which is identified in the strong CIII] emitters list. We then performed an X-ray stacking analysis on the list of strong and very strong emitters in the COSMOS field using the maps and source catalog of Civano et al. (2012). We used the CSTACK tool to separately stack the sources in the very strong and strong CIII] emitter lists after excluding the two objects with an individual detection. In the stack of galaxies in the very strong sample, the corresponding mean count rate per galaxy implies $\log L_{\rm X}(2\text{–}10\,{\rm keV}) \sim 42.6\,{\rm erg\,s^{-1}}$ at $z \sim 3$, with a noise level in the map of $\log L_{\rm X}(2\text{–}10\,{\rm keV}) \sim 42.7\,{\rm erg\,s^{-1}}$, meaning no significant detection. Conversely, in the strong sample the detection is at a 2σ level, with a count rate implying $\log L_{\rm X}(2\text{–}10\,{\rm keV}) \sim 42.9\,{\rm erg\,s^{-1}}$, with a noise level in the map of $\log L_{\rm X}(2\text{–}10\,{\rm keV}) \sim 42.6\,{\rm erg\,s^{-1}}$. The current X-ray imaging is then not deep enough to firmly confirm the presence of an X-ray source. However, the tentative 2σ detection indicates that X-ray imaging is consistent with the assumption that the very strong and strong CIII] emitting galaxies host low-luminosity AGN with X-ray luminosity, as observed at the faint end of the AGN luminosity function at these redshifts (Georgakakis et al. 2015).

In the following we further discuss the contribution of other AGN populations that are identified from spectral modeling,

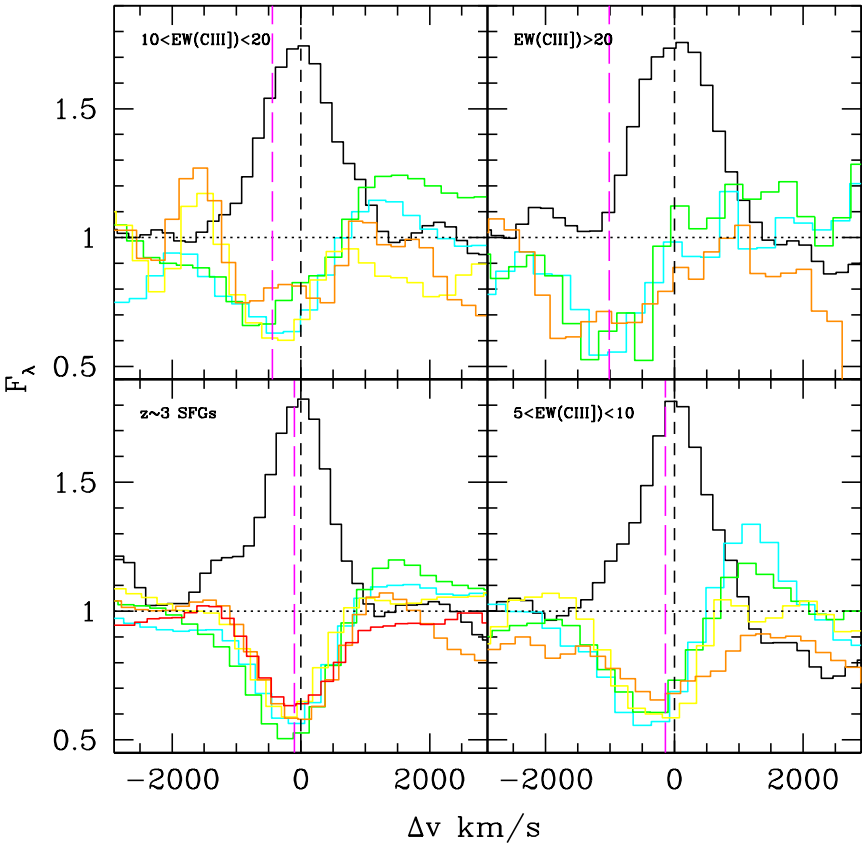

Fig. 9. Relative velocity of the main ISM absorption lines with respect to CIII]-λ1908 Å taken as systemic velocity for the SFG population and samples with increasing EW(CIII]). CIII] is plotted in black, and depending on the sample, SiII-λ1260 is drawn in cyan, SiII-λ1303 in green, CII-λ1334 in yellow, 1526 in orange, and 1670 in red. The mean outflow velocities (see text) are indicated as the long-dashed magenta lines.

beyond the AGN population that is identified from the simple criteria presented in this section.

7. Evidence that AGN quench star-formation

Several feedback-related quenching processes have been proposed, including AGN feedback, stellar wind feedback from SNe and massive stars, or environmental quenching (e.g., Croton et al. 2006; Hopkins et al. 2008; Gabor et al. 2010, 2011). Various pieces of evidence presented in this paper converge to point out that the dominant process that produces the observed quenching of star formation in strong CIII] emitters is related to AGN.

Starting from the perspective of analyzing the population of CIII] emitters, we have uncovered several important and related observed properties. We find a population of galaxies with high EW(CIII]) that reaches in excess of 20 Å (Sect. 3). These strong emitters require a strong ionizing field beyond what stellar populations can produce, but rather at a level to what can be produced by AGN (Nakajima et al. 2018). Emission line properties indicate that a fraction of these galaxies must host an AGN, as discussed in Sect. 6.4, and as extensively studied with line ratio diagnostics in Nakajima et al. (2018). Nakajima et al. (2018) used line diagnostics defined from a large grid of photoionization models including stellar populations and AGN to find that about a third of the strong and very strong emitters in VUDS require the presence of an AGN to explain the high EW(CIII]) and the position of individual emitters in line ratio diagnostic diagrams. The strongest emitters present strong outflows with a velocity above 800 km s^{-1} beyond what stellar winds can produce, and rather comparable to that of AGN (Talia et al. 2017). In addition, we find that the strongest CIII] emitters appear below the MS, and have an SFR that is lower by about 0.4 dex for the stronger emitters compared to the weak emitters. Their mean ages are almost three times older than the ages of the SFG population (Sect. 6.3). The analysis of stacked X-ray imaging presented in Sect. 6.4 further indicates a marginal detection (2σ) for the strongest CIII] emitters that is consistent with the scenario that a low-luminosity AGN with $L_X(2\text{–}10\,\mathrm{keV}) < 3 \times 10^{42}$ erg s^{-1} is hosted by those galaxies.

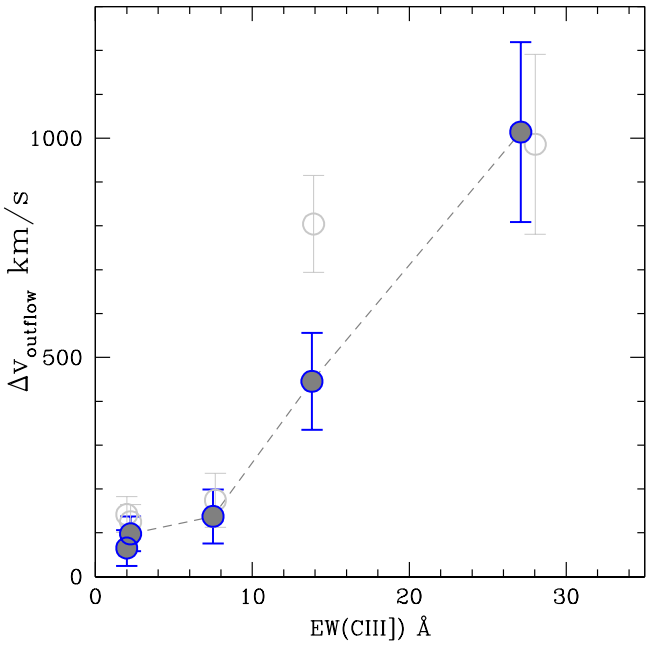

Fig. 10. Outflow velocity of ISM lines as a function of EW(CIII]) (filled symbols: velocity from the median values of the ISM lines; open symbols: mean values).

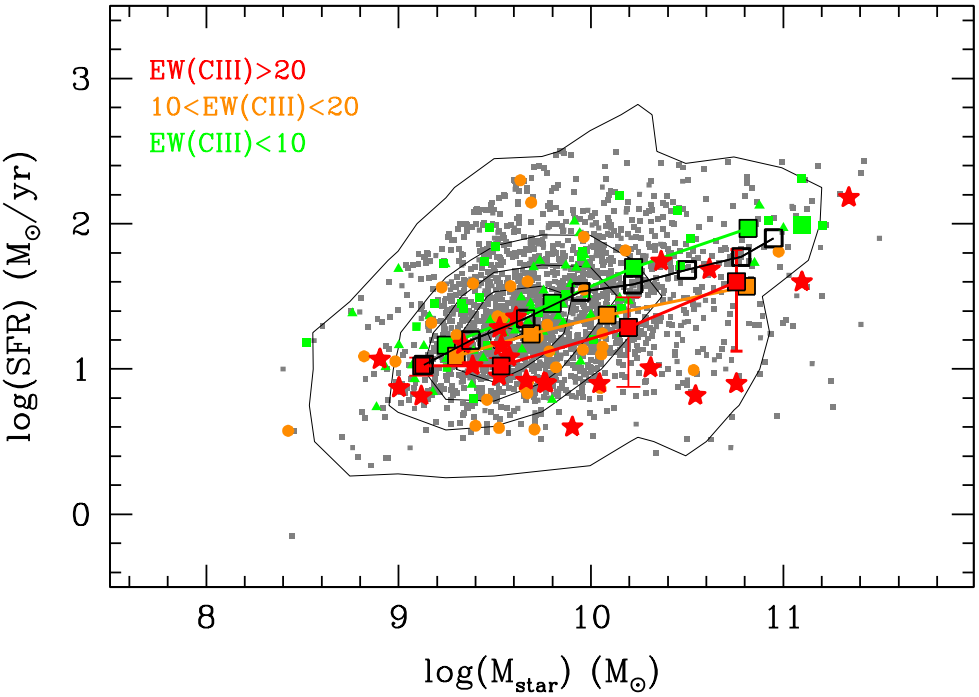

Fig. 11. Distribution of CIII] emitters with different EW(CIII]) in the $M_{\rm star}$–SFR plane. The CIII] emitters with different EW are identified by the differently colored symbols. The parent sample of star-forming galaxies at redshifts $2 < z < 3.8$ in VUDS is identified as gray symbols whose distribution is identified by the contours, and the main sequence of VUDS galaxies at $z \sim 3$ is indicated by black open squares that are connected by a thick line. We note that both the strong and very strong CIII] emitters are on average below the MS, with median values identified by the connected orange and red squares, respectively. The lower SFR of these strong CIII] emitters compared to the MS is possibly caused by a strong star formation quenching produced by AGN feedback in the host star-forming galaxies.

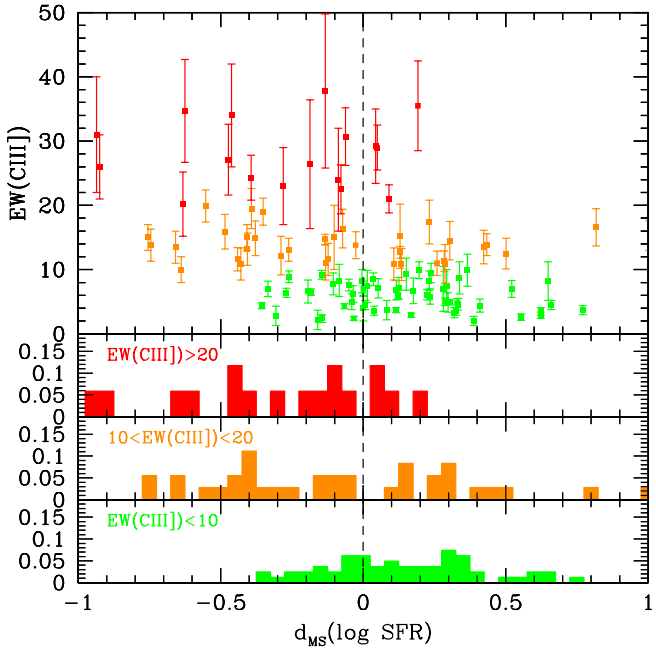

Fig. 12. *Bottom three panels*: distribution of distances in SFR from the main sequence for CIII] emitters with increasing EW(CIII]), and *top panel*: distance to the main sequence for individual CIII] emitters. As EW(CIII]) increases, the distance to the main sequence increases.

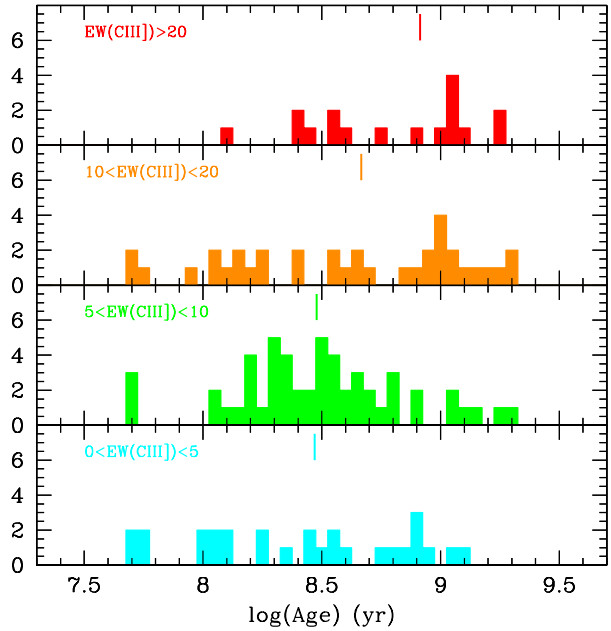

Fig. 13. Age distribution of CIII] emitters with different EW(CIII]). The median age of each population is identified by the color of the vertical lines as for their respective subsamples. The strength of the CIII] emission increases with mean age.

These observed properties all converge to favor AGN feedback as the main physical process capable of quenching the star formation in the strong and very strong CIII] emitters. In an empirical scenario, the strong ionizing field is produced by AGN that is hosted in the galaxies that are observed as CIII] emitters. The jets and winds associated with the AGN would produce strong feedback, depositing energy in the ISM, gradually removing the gas supply and effectively quenching star formation, driving those galaxies below the MS. The large age difference of up to a factor of three that is observed between the CIII] emitters and main-sequence galaxies may then indicate that the AGN feedback is taking at most a few hundred million years to operate. We therefore infer that part of the star-forming population is undergoing AGN feedback with the quenching of star formation, at any given time 10.5–12.2 Gyr after the Big Bang.

When we follow Nakajima et al. (2018) assuming that one-third of the strong and very strong CIII] emitters in the SFG sample must host an AGN, AGN feedback then concerns about one-third of the 4% of the SFG population that we identify with EW(CIII]) > 10 Å. If the duration of AGN activity

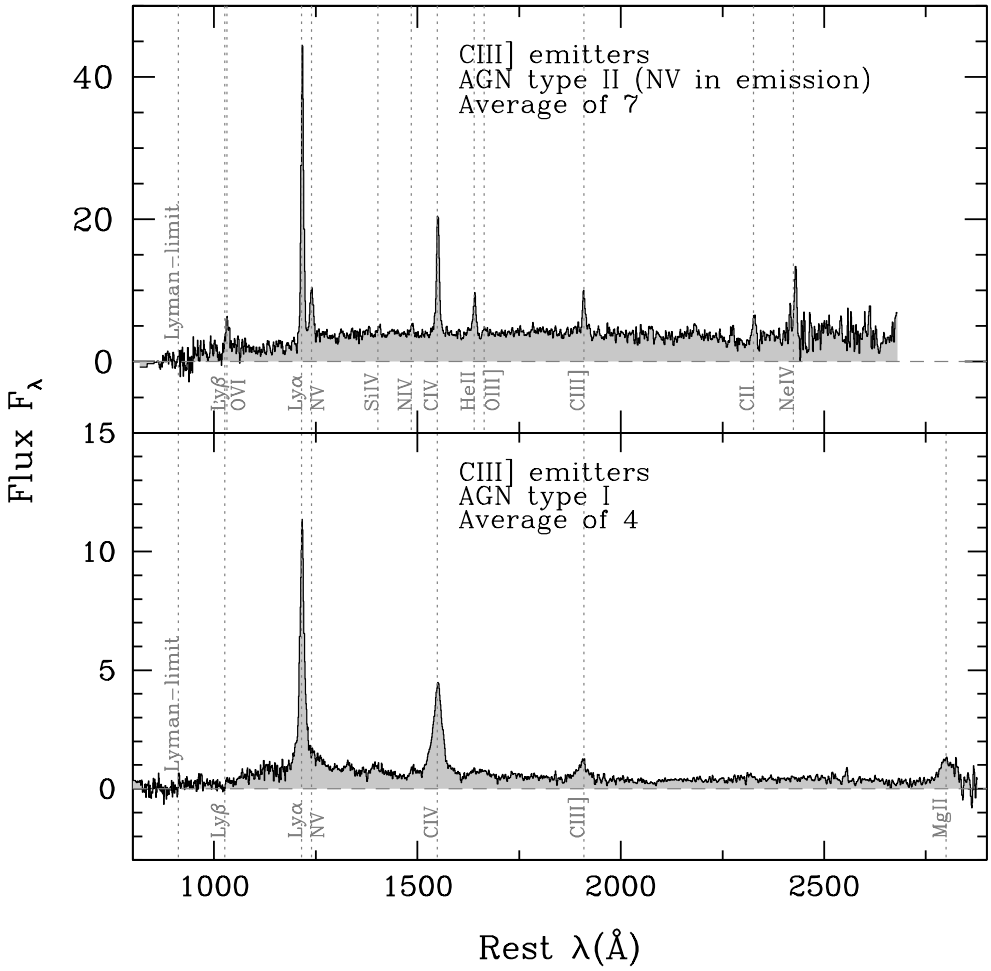

Fig. 14. Composite spectrum of four type I broad-line AGN (*bottom panel*), and seven candidate type II narrow-line AGN identified from their NV-λ1240 emission (*top panel*). See text for details on how these AGN are selected.

at an energy level required to produce galaxy-wide quenching star-formation is shorter than the cosmic time covered by our observations, the fraction of the SFG population experiencing AGN feedback and quenching could be significantly higher. We estimate the quenching timescale by assuming that SFGs subject to AGN feedback will then transform into the quiescent galaxies observed at $z \sim 2$. The volume density of quiescent galaxies with a stellar mass $M_{\rm star} > 10^{10}\,M_{\odot}$ at $z \sim 2$ is reported to be $\sim 3 \times 10^{-3}$ gal Mpc^{-3} (Brammer et al. 2011; Ilbert et al. 2013; Barro et al. 2013). From the analysis in this paper, one-third of 4% of SFGs above this mass translates into 3.3×10^{-4} gal Mpc^{-3}. For SFGs at a redshift $z \sim 3$ to transform into the right number of quiescent galaxies over a cosmic time of 1.1 Gyr to $z \sim 2$ then requires a quenching timescale $T_{\rm quench} = (3.3 \times 10^{-4}/3 \times 10^{-3}) \times 1.1$ Gyr, or about 0.35 Gyr, with a range 0.25−0.47 Gyr given the uncertainties on the AGN fraction. The effective timescale for star-formation quenching from AGN feedback is currently highly uncertain, from one hundred million years up to several hundred million years (see, e.g., Cattaneo et al. 2009; Kaviraj et al. 2011; Schawinski et al. 2014). Our results therefore seem to favor a long quenching timescale, as timescales much shorter than 0.35 Gyr would seem to overproduce quiescent galaxies by $z \sim 2$. However, these numbers are indicative and will need to be refined with improved statistics on both the fraction of SFGs subject to AGN feedback and on galaxies that are truly quiescent by $z \sim 2$. These numbers could also need to be adjusted if AGN feedback is only one of several ways to quench star formation for galaxies with $M_{\rm star} > 10^{10}\,M_{\odot}$.

The conclusions from Nakajima et al. (2018), that is, that a significant fraction of strong and very strong CIII] emitters must host an AGN, rest on the exploration of a wide range of models. It may be argued that the pure AGN models of Nakajima et al. (2018) are dust-free, a strong hypothesis. However, these models were selected because they agree better with observations of type II AGNs (e.g., Nagao et al. 2006), and the authors noted that the dividing lines they set on diagnostic diagrams to identify the preferred photoionization source are not very sensitive to dust. Moreover, for the composites of samples A and B in Nakajima et al. (2018), the authors find that their spectra are best reproduced with a hybrid model of AGN and stellar populations, where dust is included in the same manner as for the star-forming galaxy models. Alternative models that produce large EW(CIII]) may exist, and it has been suggested that strong CIII] emission might be produced in the presence of shocks (Jaskot & Ravindranath 2016), which were not considered in Nakajima et al. (2018). While we cannot exclude a contribution to CIII] emission from photoionization that is induced by shocks (e.g., in merging systems Rich et al. 2014), it does not appear to be the case that shock models are capable to produce EW(CIII]) as large as observed in the VUDS sample. Furthermore, strong shocks predict stronger CIV] emission than CIII] (Jaskot & Ravindranath 2016), which is not observed for the majority of our sample (see Nakajima et al. 2018). Therefore we conclude that AGN remain the most likely photoionization source of the strongest CIII] emitters.

Our results offer additional evidence for the co-evolution of AGN and star formation at $z \sim 2$−4. Star formation is observed

to be present coevally with AGN activity (e.g., Fabian 2012; Cimatti et al. 2013; Karman et al. 2014; Lemaux et al. 2014; Ishibashi & Fabian 2016), and this is what we witness in the strong CIII] emitters population.

8. Discussion and summary

We presented a statistical analysis of the properties of CIII]-λ1908 emitters with two aims: investigating the prevalence of CIII] emission in the star-forming galaxy population, and characterizing the properties of the population of CIII] emitters using CIII] as a diagnostic tool. To do this, we used measurements from the large sample of 3899 galaxies with $2 < z < 3.8$ in the VIMOS Ultra-Deep Survey (VUDS), .

The VUDS sample is selected from UV rest-frame luminosity ($i_{AB} \leq 25$) and provides a large unbiased sample of UV-selected star-forming galaxies in a large volume. It also minimizes cosmic variance (Le Fèvre et al. 2015) and is ideally suited to searching for CIII] emitters, exploring their properties, and deriving the appearance frequency of this emission line. Spectral line measurements including lines from Lyβ up to CIII] is made possible by the deep VIMOS spectra. In addition, spectral model fitting performed simultaneously on spectra and multi-band photometry (Thomas et al. 2017) provides physical parameters that include stellar mass, SFR, age, and dust extinction, which are used to characterize the population of CIII] emitters.

We split our sample into four categories of CIII] emitters that spanned a range from weak emitters $0 < \mathrm{EW(CIII])_{rest}} < 5$ Å to very strong emitters with an observed EW(CIII]) up to ≃40 Å for narrow-line emission spectra. Individual spectra were stacked to produce average spectral properties for each category (Figs. 4 and 5). We find that with increasing EW(CIII]), emission lines appear that require a higher ionizing potential. The strongest emitters show NV-λ1240, SiII-λ1309, SiIV-λ1403, NIV]-λ1485, CIV-λ1549, HeII-λ1640, OIII]-λ1663, NIII]-λ1750, and SiIII]-λ1888 (Fig. 5).

We find a correlation between Lyα emission and CIII] emission (Fig. 6), but with a large dispersion because we find strong CIII] emitters with Lyα in absorption, or strong Lyα emission and no or weak CIII]. We explored the properties of the CIII] population and find that EW(CIII]) weakly increases with near-UV luminosity L_{NUV}, and that the total size of galaxies decreases as EW(CIII]) increases (Fig. 8).

From the complete VUDS sample we computed the distribution of EW(CIII]) (Fig. 7) and find that about 24% of the population shows some sign of CIII] emission. A first visual impression was already given in the Fig. 10 of Le Fèvre et al. (2015), as CIII] can be followed clearly from the 2D spectra image of the whole VUDS sample. We quantified this statement, finding that 20% of the population show weak emission with $3 < \mathrm{EW(CIII])} < 10$ Å, 4% have an $\mathrm{EW(CIII])} > 10$ Å, and 1.2% present very strong emission with $\mathrm{EW(CIII])} > 20$ Å. We find that the probability for LAE to show CIII] in emission with an $\mathrm{EW(CIII])} > 3$ Å is 42%.

While the presence of CIII] emission therefore appears rather frequent, we note that the vast majority of CIII] emitters are weak emitters, which means that this line is difficult to identify, except for the ∼4% of the population that have an $\mathrm{EW(CIII])} > 10$ Å. We therefore cannot expect to rely on CIII] emission alone as a means to measure the spectroscopic redshifts of galaxies in a complete sample of SFGs. Redshift measurements of UV-rest spectra without Lyα emission will still need to rely on a combination of the most prominent spectral features. Typically, in addition of CIII], lines such as CIV, HeII, the continuum break at and below Lyα, and hard-to-detect absorption features can jointly serve to eliminate degenerate redshift solutions.

The fraction of strong CIII] emitters is expected to increase at higher redshifts toward the epoch of HI reionization (EoR) at $z > 6$, only in the presence of a stronger ionizing field than observed in our sample at $2 < z < 3.8$, together with very low metallicity. Such conditions may exist in the lower luminosity galaxies in our sample (Sect. 6.1), and such galaxies may be prevalent in the EoR. Some analogs to those expected in the EoR have been discussed in Amorín et al. (2017). It is well possible that as the population of forming galaxies becomes younger, with lower stellar mass, and lower metallicity, the fraction of objects with strong CIII] emission in the EoR becomes higher than in our sample at $z \sim 3$. This may be the case for the very first generation of stars in the first galaxies (Nakajima et al. 2018). Exactly how this fraction of strong emitters will increase at higher redshifts remains to be investigated.

The main result from this paper is a coherent set of observational evidence that indicates that AGN feedback acts on the population of strong CIII] emitters. Upon examination of spectral features, we identified four galaxies with broad emission lines, their quasar-like spectra clearly powered by strong AGN. We identified seven objects in which the NV-λ1240 narrow emission line $\mathrm{EW(NV)} > 10$ Å was recognized as a potential tracer of AGN activity. The most striking observational results include the clear evidence for strong outflows up to $\sim 1000\,\mathrm{km\,s^{-1}}$ for the strongest CIII] emitters, and increasingly lower SFR in the SFR–M_{star} plane as EW(CIII]) increases. Such strong outflows require energy levels beyond what stellar winds are capable of producing on a galaxy scale, but they are consistent with being powered by AGN (e.g., Harrison et al. 2012; Cimatti et al. 2013; Förster Schreiber et al. 2014; Brusa et al. 2015). The distribution of CIII] emitters in the stellar mass vs. SFR plane around the main sequence of star-forming galaxies is investigated in Fig. 11. Our analysis shows that the strong and very strong emitters are on average below the MS, indicating that the star formation is quenched in these galaxies, and the SFR decreases when EW(CIII]) increases. From X-ray data stacking, we find a marginal 2σ detection that is consistent with low-luminosity AGN with $L_X(2\text{–}10\,\mathrm{keV}) \sim 42.9\,\mathrm{erg\,s^{-1}}$ for the strong and very strong CIII] emitters, as observed at the faint end of the AGN luminosity function at these redshifts (Georgakakis et al. 2015).

The physical origin of CIII] emission in relation to the prevalent ionizing field was investigated in Nakajima et al. (2018). From the data presented here, Nakajima et al. (2018) derived various line ratio diagnostics on the basis of a wide range of photoionizing models by combining CIII]-λ1908 with other emission lines such as CIV-λ1549, HeII-λ1640, and OIII]-λ1664. The authors found that the strong and very strong CIII] emitters must host an AGN in order to produce the large EW(CIII]) and observed line ratios.

Alternative models, for instance, those that invoke shocks, do not seem capable of producing an EW(CIII]) as large as observed in VUDS, and strong shocks predict high CIV]/CIII] ratios (Jaskot & Ravindranath 2016), which are not observed in the bulk of our sources. The spectral analysis of Nakajima et al. (2018) reinforces our proposed scenario with strong AGN-driven quenching of star-formation. Without AGN, it seems unlikely that conditions with the high star-formation activity are met that is required to produce strong CIII] and the observed line ratios while at the same time producing strong outflows and driving galaxies off the MS. We instead conclude that it is more realistic

that AGN and star formation activity act together to produce the observed properties of CIII] emitters.

The signature of AGN has previously been reported in SFGs at and beyond the peak in SFRD (e.g., Cimatti et al. 2013; Genzel et al. 2014; Talia et al. 2012, 2017; Karman et al. 2014). The regulation of mass growth from the quenching of star formation has been proposed to support an evolutionary path that gradually transforms SFGs at the highest redshifts into quiescent galaxies observed at $z \sim 1-2$ (Barro et al. 2013). In this context, AGN feedback was identified in numerical simulations as the prime contender for the quenching of star formation (Hopkins et al. 2006, 2008). The results presented in this paper bring further evidence of the presence of AGN in SFGs at a key epoch of mass build-up in galaxies

The properties of CIII] emitters are consistent with an empirical scenario in which CIII] emitting galaxies with increasing EW host an increasingly larger fraction of AGN that produces the strong ionizing field that is required to ionize CIII] to the observed levels. These AGN drive the strong observed outflows, and in the end, they quench star formation in the host galaxies to produce the observed location of CIII] emitters in the SFR–$M_{\rm star}$ plane. The age of the stellar populations of the stronger emitters is found to be about three times that of the weak emitters, at ∼0.8 vs. 0.3 Gyr, respectively. This may be an indication that the strongest emitters were the first to experience AGN feedback and the associated quenching. We find that quenching timescales of $\sim 0.25-0.5 \times 10^8$ years are required to transform SFGs with $M_{\rm star} > 10^{10}\,M_{\odot}$ into the volume density of quiescent galaxies observed at $z \sim 2$ (Brammer et al. 2011; Ilbert et al. 2013; Barro et al. 2013).

We conclude that the co-evolution of stellar populations and AGN is a key ingredient of the star formation evolution and mass build-up in galaxies at these early times. Future experiments assembling larger datasets are required to investigate whether the AGN feedback and quenching we identified in the redshift range of this paper and beyond is mass dependent.

The results presented here indicate that large comprehensive spectroscopic surveys are required that have the power to identify galaxy populations that may appear to be rare but provide important clues on the first phases of galaxy assembly. Our study paves the way for a systematic use of spectral line properties and diagnostics from the UV to optical rest-frame for future investigations that use next-generation facilities such as the *James Webb* Space Telescope and ELTs.

Acknowledgements. This work is supported by funding from the European Research Council Advanced Grant ERC–2010–AdG–268107–EARLY and by INAF Grants PRIN 2010, PRIN 2012 and PICS 2013. AC, OC, MT, and VS acknowledge the grant MIUR PRIN 2015. This work is based on data products made available at the CESAM data center, Laboratoire d'Astrophysique de Marseille, France.

References

Alexandroff, R., Strauss, M. A., Greene, J. E., et al. 2013, MNRAS, 435, 3306
Amorín, R., Fontana, A., Pérez-Montero, E., et al. 2017, Nat. Astron., 1, 0052
Assef, R. J., Kochanek, C. S., Brodwin, M., et al. 2010, ApJ, 713, 970
Barro, G., Faber, S. M., Pérez-González, P. G., et al. 2013, ApJ, 765, 104
Best, P. N., Röttgering, H. J. A., & Longair, M. S. 2000, MNRAS, 311, 23
Bongiorno, A., Merloni, A., Brusa, M., et al. 2012, MNRAS, 427, 3103
Bournaud, F., Chapon, D., Teyssier, R., et al. 2011, ApJ, 730, 4
Bouwens, R. J., Illingworth, G. D., Oesch, P. A., et al. 2015, ApJ, 803, 34
Bradač, M., Garcia-Appadoo, D., Huang, K.-H., et al. 2017, ApJ, 836, L2
Brammer, G. B., Whitaker, K. E., van Dokkum, P. G., et al. 2011, ApJ, 739, 24
Brusa, M., Bongiorno, A., Cresci, G., et al. 2015, MNRAS, 446, 2394
Bundy, K., Georgakakis, A., Nandra, K., et al. 2008, ApJ, 681, 931
Capak, P. L., Carilli, C., Jones, G., et al. 2015, Nature, 522, 455
Carilli, C. L., & Walter, F. 2013, ARA&A, 51, 105
Cassata, P., Le Fèvre, O., Charlot, S., et al. 2013, A&A, 556, A68
Cassata, P., Tasca, L. A. M., Le Fèvre, O., et al. 2015, A&A, 573, A24
Cattaneo, A., Faber, S. M., Binney, J., et al. 2009, Nature, 460, 213
Chiappetti, L., Clerc, N., Pacaud, F., et al. 2013, MNRAS, 429, 1652
Cimatti, A., Brusa, M., Talia, M., et al. 2013, ApJ, 779, L13
Civano, F., Elvis, M., Brusa, M., et al. 2012, ApJS, 201, 30
Civano, F., Marchesi, S., Comastri, A., et al. 2016, ApJ, 819, 62
Croton, D. J., Springel, V., White, S. D. M., et al. 2006, MNRAS, 365, 11
De Barros, S., Pentericci, L., Vanzella, E., et al. 2017, A&A, 608, A123
Du, X., Shapley, A. E., Martin, C. L., & Coil, A. L. 2017, ApJ, 838, 63
Dubois, Y., Gavazzi, R., Peirani, S., & Silk, J. 2013, MNRAS, 433, 3297
Erb, D. K., Pettini, M., Shapley, A. E., et al. 2010, ApJ, 719, 1168
Fabian, A. C. 2012, ARA&A, 50, 455
Förster Schreiber, N. M., Genzel, R., Newman, S. F., et al. 2014, ApJ, 787, 38
Gabor, J. M., Davé, R., Finlator, K., & Oppenheimer, B. D. 2010, MNRAS, 407, 749
Gabor, J. M., Davé, R., Oppenheimer, B. D., & Finlator, K. 2011, MNRAS, 417, 2676
Garilli, B., Fumana, M., Franzetti, P., et al. 2010, PASP, 122, 827
Genzel, R., Förster Schreiber, N. M., Rosario, D., et al. 2014, ApJ, 796, 7
Georgakakis, A., Aird, J., Buchner, J., et al. 2015, MNRAS, 453, 1946
Guaita, L., Talia, M., Pentericci, L., et al. 2017, A&A, 606, A19
Hainline, K. N., Shapley, A. E., Greene, J. E., & Steidel, C. C. 2011, ApJ, 733, 31
Hainline, K. N., Shapley, A. E., Greene, J. E., et al. 2012, ApJ, 760, 74
Hanuschik, R. W. 2003, A&A, 407, 1157
Harrison, C. M., Alexander, D. M., Swinbank, A. M., et al. 2012, MNRAS, 426, 1073
Hathi, N. P., Le Fèvre, O., Ilbert, O., et al. 2016, A&A, 588, A26
Heckman, T. M., Borthakur, S., Overzier, R., et al. 2011, ApJ, 730, 5
Hoag, A., Bradacč, M., Trenti, M., et al. 2017, Nat. Astr., 1, 0091
Hopkins, P. F., Hernquist, L., Cox, T. J., et al. 2006, ApJS, 163, 1
Hopkins, P. F., Hernquist, L., Cox, T. J., & Kereš, D. 2008, ApJS, 175, 356
Ilbert, O., McCracken, H. J., Le Fèvre, O., et al. 2013, A&A, 556, A55
Ishibashi, W., & Fabian, A. C. 2016, MNRAS, 463, 1291
Jaskot, A. E., & Ravindranath, S. 2016, ApJ, 833, 136
Karman, W., Caputi, K. I., Trager, S. C., Almaini, O., & Cirasuolo, M. 2014, A&A, 565, A5
Kaviraj, S., Schawinski, K., Silk, J., & Shabala, S. S. 2011, MNRAS, 415, 3798
Kehrig, C., Vílchez, J. M., Pérez-Montero, E., et al. 2015, ApJ, 801, L28
Le Fèvre, O., Saisse, M., Mancini, D., et al. 2003, SPIE Conf. Ser., 4841, 1670
Le Fèvre, O., Tasca, L. A. M., Cassata, P., et al. 2015, A&A, 576, A79
Lemaux, B. C., Lubin, L. M., Shapley, A., et al. 2010, ApJ, 716, 970
Lemaux, B. C., Le Floc'h, E., Le Fèvre, O., et al. 2014, A&A, 572, A90
Luo, B., Brandt, W. N., Xue, Y. Q., et al. 2017, ApJS, 228, 2
Maio, U., Petkova, M., De Lucia, G., & Borgani, S. 2016, MNRAS, 460, 3733
Marchesi, S., Civano, F., Elvis, M., et al. 2016, ApJ, 817, 34
Matsuoka, K., Nagao, T., Maiolino, R., Marconi, A., & Taniguchi, Y. 2009, A&A, 503, 721
Moster, B. P., Somerville, R. S., Newman, J. A., & Rix, H.-W. 2011, ApJ, 731, 113
Nagao, T., Maiolino, R., & Marconi, A. 2006, A&A, 447, 863
Nakajima, K., Schaerer, D., Le Fèvre, O., et al. 2018, A&A, 612, A94
Oesch, P. A., Brammer, G., van Dokkum, P. G., et al. 2016, ApJ, 819, 129
Ouchi, M., Shimasaku, K., Akiyama, M., et al. 2008, ApJS, 176, 301
Pallottini, A., Ferrara, A., Bovino, S., et al. 2017, MNRAS, 471, 4128
Pentericci, L., Fontana, A., Vanzella, E., et al. 2011, ApJ, 743, 132
Pentericci, L., Vanzella, E., Fontana, A., et al. 2014, ApJ, 793, 113
Pentericci, L., Carniani, S., Castellano, M., et al. 2016, ApJ, 829, L11
Ribeiro, B., Le Fèvre, O., Tasca, L. A. M., et al. 2016, A&A, 593, A22
Ribeiro, B., Le Fèvre, O., Cassata, P., et al. 2017, A&A, 608, A16
Rich, J. A., Kewley, L. J., & Dopita, M. A. 2014, ApJ, 781, L12
Rigby, J. R., Bayliss, M. B., Gladders, M. D., et al. 2015, ApJ, 814, L6
Robertson, B. E., Ellis, R. S., Furlanetto, S. R., & Dunlop, J. S. 2015, ApJ, 802, L19
Schaerer, D. 2003, A&A, 397, 527
Schawinski, K., Urry, C. M., Simmons, B. D., et al. 2014, MNRAS, 440, 889
Schmidt, K. B., Treu, T., Bradač, M., et al. 2016, ApJ, 818, 38
Schmidt, K. B., Huang, K.-H., Treu, T., et al. 2017, ApJ, 839, 17
Scodeggio, M., Franzetti, P., Garilli, B., et al. 2005, PASP, 117, 1284
Shapley, A. E., Steidel, C. C., Pettini, M., & Adelberger, K. L. 2003, ApJ, 588, 65
Shibuya, T., Ouchi, M., Harikane, Y., et al. 2018, PASJ, 70, S15
Silk, J., & Rees, M. J. 1998, A&A, 331, L1
Sobral, D., Matthee, J., Darvish, B., et al. 2015, ApJ, 808, 139

Stark, D. P., Ellis, R. S., Bunker, A., et al. 2009, ApJ, 697, 1493
Stark, D. P., Ellis, R. S., Chiu, K., Ouchi, M., & Bunker, A. 2010, MNRAS, 408, 1628
Stark, D. P., Richard, J., Siana, B., et al. 2014, MNRAS, 445, 3200
Stark, D. P., Richard, J., Charlot, S., et al. 2015, MNRAS, 450, 1846
Steidel, C. C., Rudie, G. C., Strom, A. L., et al. 2014, ApJ, 795, 165
Stern, D., Dey, A., Spinrad, H., et al. 1999, AJ, 117, 1122
Stroe, A., Sobral, D., Matthee, J., Calhau, J., & Oteo, I. 2017, MNRAS, 471, 2558
Talia, M., Mignoli, M., Cimatti, A., et al. 2012, A&A, 539, A61
Talia, M., Brusa, M., Cimatti, A., et al. 2017, MNRAS, 471, 4527
Taniguchi, Y., Kajisawa, M., Kobayashi, M. A. R., et al. 2015, ApJ, 809, L7
Tasca, L. A. M., Le Fèvre, O., Hathi, N. P., et al. 2015, A&A, 581, A54
Tasca, L. A. M., Le Fèvre, O., Ribeiro, B., et al. 2017, A&A, 600, A110
Thacker, R. J., Scannapieco, E., & Couchman, H. M. P. 2006, ApJ, 653, 86
Thomas, R., Le Fèvre, O., Scodeggio, M., et al. 2017, A&A, 602, A35
Treu, T., Schmidt, K. B., Trenti, M., Bradley, L. D., & Stiavelli, M. 2013, ApJ, 775, L29
Vanden Berk, D. E., Richards, G. T., Bauer, A., et al. 2001, AJ, 122, 549
Vanzella, E., Pentericci, L., Fontana, A., et al. 2011, ApJ, 730, L35
Villar-Martin, M., Tadhunter, C., & Clark, N. 1997, A&A, 323, 21
Zackrisson, E., Binggeli, C., Finlator, K., et al. 2017, ApJ, 836, 78

Appendix A: Additional tables

Table A.1. Equivalent width of emission lines in stacked CIII] spectra.

Line-λ	Sample							
	EW(CIII]) ≥ 20 Å		10 ≤ EW(CIII]) < 20 Å		5 ≤ EW(CIII]) < 10		AGN type II	
	EW (Å)	Flux (relative to CIII)	EW (Å)	Flux (relative to CIII)	EW (Å)	Flux (relative to CIII)	EW (Å)	Flux (relative to CIII)
Lyα	71.7^{+4}_{-5}	4.6 ± 0.07	$58.8^{+7.0}_{-3.5}$	6.4 ± 0.04	$30.3^{+2.3}_{-1.5}$	5.2 ± 0.2	98.8^{+3}_{-3}	6.25 ± 0.06
NV-λ1240 Å	$0.9^{+0.3}_{-0.3}$	0.05 ± 0.02	$0.3^{+0.15}_{-0.15}$	0.02 ± 0.01	–	–	19.1^{+2}_{-2}	1.31 ± 0.1
SiII-λ1309 Å	$0.6^{+0.2}_{-0.2}$	0.07 ± 0.02	$0.2^{+0.15}_{-0.15}$	0.04 ± 0.02	–	–	$1.7^{+0.4}_{-0.4}$	0.12 ± 0.04
SiIV-λ1403 Å	$1.4^{+0.2}_{-0.2}$	0.13 ± 0.03	$0.1^{+0.15}_{-0.15}$	0.02 ± 0.02	–	–	$1.9^{+0.4}_{-0.5}$	0.14 ± 0.04
NIV-λ1485 Å	$2.2^{+0.3}_{-0.3}$	0.19 ± 0.02	$0.6^{+0.1}_{-0.1}$	0.08 ± 0.02	–	–	$2.5^{+0.5}_{-0.5}$	0.19 ± 0.05
CIV-λ1549 Å	$4.4^{+0.6}_{-0.5}$	0.31 ± 0.03	$2.4^{+0.5}_{-0.2}$	0.36 ± 0.02	$0.1^{+0.2}_{-0.3}$	0.01 ± 0.1	$38.8^{+2.0}_{-2.1}$	3.00 ± 0.08
HeII-λ1640 Å	$4.3^{+0.7}_{-0.4}$	0.27 ± 0.03	$3.2^{+0.5}_{-0.3}$	0.49 ± 0.03	$1.7^{+0.2}_{-0.2}$	0.3 ± 0.06	$11.7^{+1.0}_{-0.5}$	0.92 ± 0.06
OIII]-λ1664 Å	$5.5^{+0.6}_{-0.5}$	0.27 ± 0.03	$1.4^{+0.4}_{-0.3}$	0.14 ± 0.02	$0.7^{+0.2}_{-0.2}$	–	$1.7^{+0.6}_{-0.5}$	0.13 ± 0.05
NIII-λ1750 Å	$1.1^{+0.2}_{-0.2}$	0.07 ± 0.03	$0.4^{+0.2}_{-0.2}$	0.04 ± 0.02	–	–	$1.5^{+0.7}_{-0.6}$	0.13 ± 0.06
SiIII-λ1888 Å	$5.0^{+0.4}_{-0.3}$	0.18 ± 0.12	$4.0^{+0.4}_{-0.5}$	0.31 ± 0.10	–	–	$2.5^{+0.9}_{-0.8}$	0.19 ± 0.02
CIII]-λ1908 Å	$23.5^{+1.6}_{-1.8}$	1 ± 0.05	$11.1^{+1.2}_{-1.1}$	1 ± 0.04	$7.1^{+1.3}_{-1.1}$	1 ± 0.15	$13.2^{+1.2}_{-1.0}$	1.0 ± 0.09
UV slope β	−1.76 ± 0.08		−1.61 ± 0.03		−1.35 ± 0.02		0.09 ± 0.02	
$\Delta V_{\rm outflow}$ km s^{-1}	1014 ± 205		445 ± 110		137 ± 61		–	

Table A.2. Equivalent width of emission lines in stacked CIII] spectra.

Line-λ	Sample			
	SFGs 2 < z < 3		SFGs 3 < z < 4	
	EW (Å)	Flux (relative to CIII)	EW (Å)	Flux (relative to CIII)
Lyα	$7.9^{+1.3}_{-1.3}$	3.5 ± 0.1	$14.8^{+1.5}_{-1.2}$	4.5 ± 0.12
CIV-λ1549 Å	$2.78^{+0.11}_{-0.06}$	−2.1 ± 0.05	$2.84^{+0.15}_{-0.05}$	−1.2 ± 0.05
CIII]-λ1908 Å	$2.0^{+0.2}_{-0.2}$	1 ± 0.05	$2.24^{+0.3}_{-0.2}$	1 ± 0.05
UV slope β	−0.94 ± 0.02		−0.92 ± 0.02	
$\Delta V_{\rm outflow}$ km s^{-1}	65 ± 41		98 ± 40	